Chapter 21
Computational Studies of Adsorption of Toxic Molecules and Anions on the Surface of Doped and Functionalized Carbon Nanotubes

V. Borysiuk, S. G. Nedilko, Yu. Hizhnyi, and A. Shyichuk

21.1 Introduction

Removal of toxic molecules and ions of heavy metals from environment is an urgent technological requirement of human civilization. One of the most promising methods of such kind of removal is adsorption of toxic molecules by artificial adsorbents [1, 2]. The search for new adsorbent materials which can allow economically efficient schemes of such removal is a topical research task [1, 3].

Materials based on carbon nanostructured materials, in particular carbon nanotubes (CNTs), are considered as very promising candidates for such application [1, 2, 4, 5]. Among other adsorbent materials, the CNTs are characterized by a number of advantages, most notably large surface area and generally high adsorption capability of carbon surface for many toxic compounds [1, 3].

Carbon nanotubes (CNTs) are intensively studied at present time as promising materials for gas sensors [6–10]. Specific properties of CNT-based materials allow elaboration of efficient gas sensors with sensitivity in the ppb region [6, 11, 12] and with several additional advantages, such as low dimensions, fast response, good reversibility at ambient temperature, and low power consumption.

Computational studies of adsorptions of various molecules on the surfaces of carbon nanostructures, in particular CNTs and graphene, have become a powerful tool for quantitative description of adsorption characteristics of real carbon nanomaterials [13]. Computational approaches in the studies of adsorption of toxic molecules and anions on the CNT surface have been recognized as having high

V. Borysiuk (✉) · S. G. Nedilko · Y. Hizhnyi
Taras Shevchenko National University of Kyiv, Kyiv, Ukraine

A. Shyichuk
Department of Rare Earth, Faculty of Chemistry, Adam Mickiewicz University, Poznań, Poland

O. Fesenko, L. Yatsenko (eds.), *Nanophotonics, Nanooptics, Nanobiotechnology, and Their Applications*, Springer Proceedings in Physics 222,
https://doi.org/10.1007/978-3-030-17755-3_21

predictive power. Since computational modeling can predict several important physical and chemical properties of the sensor materials, the computations themselves can evaluate the prospects for removal of toxic molecules from the environment, as well as for elaboration of novel gas sensors [14–17]. Adsorption of several types of molecules of industrially important toxic gases on the B- or N-CNTs was treated so far in the density functional theory (DFT)-based electronic structure calculations. In particular, such studies were reported for carbon monoxide (CO) [18–20], nitrogen dioxide (NO_2) [18, 19], chlorine (Cl_2) [20], formaldehyde (HCOH) [17], methanol (CH_3OH), and ammonia (NH_3) [19, 21].

Hydrogen halide gases HX (X = F, Cl, Br) are widely used in the industry as reagents (see [22]) and also are produced as byproducts in many industrial applications (see [23–26]). At the same time, these gases are very toxic and harmful for biological organisms even at low concentrations [22, 27]. Majority of electrochemical gas sensors of hydrogen halides available on the market are relatively expensive and their detection limit usually does not exceed the ppm level [28]. Elaboration of novel, more efficient, and sensitive sensors of hydrogen halide gases is an important present-day task.

Compounds of hexavalent ions of heavy metals M(VI), in particular Cr(VI), are widely spread industrial pollutants, and at the same time, they are very harmful to living bodies [29–31]. Therefore, there is a strong technological need to remove such compounds from industrial waste as well as from the environment [32, 33]. The properties of CNTs as adsorption materials for Cr(VI) compounds have been studied over the last decade [4, 32, 34–38] and it was found that these materials are very promising for the efficient removal of Cr(VI) compounds from the environment [2, 32, 35–37].

However, despite of a large volume of accumulated experimental data, there is a considerable lack of understanding of Cr(VI)-on-CNTs adsorption mechanisms at the single-molecule level. In particular, the peculiarities of chemical bonding between the most common types of Cr(VI) anions and the CNT surface still remain unclear.

Adsorption models developed in the mentioned above research papers usually employ analogies with adsorption of molecules on a carbon surface without explicit consideration of specific CNT structures. However, it is well-known that carbon surface of CNTs (particularly low-diameter ones) may be significantly curved, and this feature determines their distinctive adsorption properties [39].

Chromium is the 21st most abundant element in the earth's crust [40], and its valance state can range from -2 to $+6$, but it is generally found as trivalent Cr(III) and hexavalent chromium Cr(VI) in natural environments.

Trivalent chromium occurs naturally in many vegetables, fruits, meat, grains and is often added to vitamins as a dietary supplement, whereas Cr(VI) most often produced by industrial processes and mining of chromium ore, is an indicator of the environmental contamination. The main industries that contribute to water pollution by Cr(VI) are leather production, mining, electroplating, textile dyeing, metal finishing, wood manufacturing, nuclear power plants, electrical and electronic

equipment manufacturing, catalysis [41–46]. For this reason, hexavalent chromium is among very common environmental pollutants.

Most of the Cr(III) compounds are sparingly soluble in water, whereas the majority of Cr(VI) compounds are highly soluble. In addition, Cr(III) is several times less toxic than Cr(VI) [47]. The tolerance limit for Cr(VI) for discharge into inland surface waters is 0.1 mg/L and 0.05 mg/L in potable water.

The effect of hexavalent chromium on humans can occur not only due to use of contaminated water but also by inhalation of contaminated air and the contact of evaporation with the skin. Hexavalent chromium, Cr(VI), are dangerous to humans at all ways of interaction, even with short-term impact. The above determine the relevance for investigation of the adsorption mechanisms of chromium-containing anions, first of all those containing Cr(VI), and shows the need to study these mechanisms both in gas and water environments. Chromium(VI) generally exists in monomeric ($HCrO_4^-$ and CrO_4^{2-}) or biomeric state ($Cr_2O_7^{2-}$) [48]. The dependency of concentration of these species on the pH and concentration of Cr(VI) solution are presented in Figs. 21.1 and 21.2, respectively.

It is evident (Fig. 21.2) that CrO_4^{2-} predominates above pH 6.5 and $HCrO_4^-$ dominates in the pH range of 1–6.5.

The above description shows the need to study the mechanisms of adsorption on the surface of carbon materials of such molecular chromium groups as CrO_4^{2-}, $HCrO_4^-$, and $Cr_2O_7^{2-}$.

Besides Cr(VI)-containing ions, the DFT-based calculations provide an opportunity to study the adsorption mechanisms of molecules with other hexavalent ions Mo(VI) and W(VI). These ions are isovalent to Cr(VI), which, however, does not determine the identity of the adsorption characteristics of corresponding molecules and anions on the surfaces of various carbon nanostructured materials.

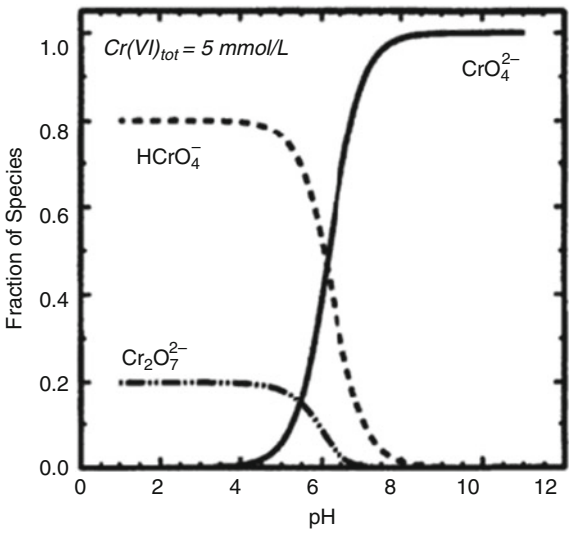

Fig. 21.1 Distribution of Cr(VI) species as a function of pH [48]

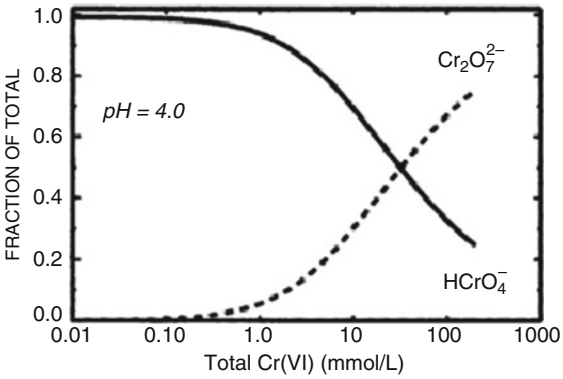

Fig. 21.2 Fraction of $HCrO_4^-$ and $Cr_2O_7^{2-}$ at pH 4 as a function of total Cr(VI) concentration [48]

21.2 Fundamentals of the Structural and Electronic Properties of Carbon Nanotubes

It is well-known that the first observation of the structure of multi-walled carbon nanotubes was in 1991 [49]; however, there are a number of works in which the evidence is provided for an earlier discovery of the CNTs. In 1976, it was clearly shown the existence of hollow carbon fibers of nanometer diameters [50]. In 1987, the US patent [51] was issued for the production of discrete cylindrical carbon fibers with a constant diameter in the range of 3.5–70 nm and a length that is 102 times greater than the diameter. In 1991, the multiwalled carbon nanotubes contained in arc discharge were registered and investigated [49]. Methods for the synthesis of the single-walled carbon nanotubes were also described [52, 53].

Carbon nanotubes have a hollow cylindrical structure with a diameter of 1 to several 10s of nanometers and a length of up to hundreds of micrometers, consisting of one or more hexa-honalnyh graphite planes (graphene sheets) rolled into a tube and ending generally hemispherical surface, which can be seen as half fullerene molecule [53]. For example, CNT(10,10) ends with a half-fullerene C_{240}. The CNT can also have open ends after oxidation [54]. Depending on the number of graphene layers, the nanotubes can be single-walled (SWCNT) or multiwalled (MWCNT). The ideal SWCNT can be represented as a graphene sheet (hexagonal layer of carbon atoms) rolled up into the cylinder without the presence of any seams.

Since the microscopic structure of SWCNT is closely related to graphene, the tubes are usually denoted in terms of graphene lattice vectors, it can be obtained geometrically by curling strips of graphene. The geometry of the SWCNT is completely determined by a pair of indices (n,m) indicating the relative position $C_h = na_1 + ma_2$ pair of atoms of graphene strips, which, upon the tube formation of, are superimposed on each other (a_1 and a_2 are the basis vectors of the hexagonal layer).

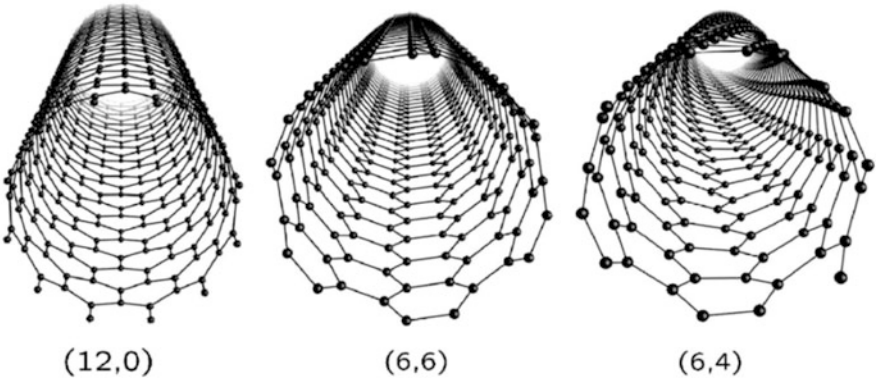

Fig. 21.3 Atomic structures of (12,0) zigzag, (6,6) armchair, and (6,4) chiral nanotubes [55]

This chiral vector C_h defines the circumference of the tube. The diameter d_t of the nanotube can thus be calculated from:

$$d_t = |C_h| / \pi \tag{21.1}$$

The chiral vector C_h uniquely defines a particular (n,m) of the tube, as well as its chiral angle θ, which is the angle between C_h and a_1.

Nanotubes of the (n,n) type ($\theta = 30°$) are called armchair tubes, because they exhibit an armchair pattern along the circumference. Such tubes display carbon-carbon bonds perpendicular to the nanotube axis. Both zigzag and armchair nanotubes are achiral tubes, in contrast with general (n,$m \neq n \neq 0$) chiral ones (Fig. 21.3).

The geometry of the graphene lattice and the chiral vector determine not only the diameter of the CNT but also the unit cell and its number of carbon atoms. The smallest graphene lattice vector T perpendicular to C_h defines the translational period t along the tube axis. The lattice vector T can also be expressed in terms of the basis vectors a_1 and a_2 as $T = t_1 a_1 + t_2 a_2$. Using $C_h, \cdot T = 0$, the expressions for t_1 and t_2 are represented by:

$$t_1 = (2m + n) / N_R, \quad t_2 = -(2n + m) / N_R \tag{21.2}$$

where N_R is the greatest common divisor of $(2m + n)$ and $(2n + m)$. The number of carbon atoms per unit cell N_C can also be expressed as a function of n and m:

$$N_C = 4\left(n^2 + nm + m^2\right) / N_R \tag{21.3}$$

As in the case of bulk crystalline solids, in CNTs, the appearance of "native" defects, which are formed in the places of the transformation of a part of hexagonal cycles into five- and seven-circular cycles with the formation of rings of nanotubes,

may occur. Defects can also be external: introduced accidentally due to the manufacturing process or which are specially incorporated to modify the properties of the nanotubes. The appearance of defects in CNT leads to the bend of the tube, the change of the chirality vector and its diameter, the change in the relation with adjacent tubes in the beam, and, consequently, the change in the properties of the CNTs.

Carbon nanotubes are known for their special electronic properties due to the nature of the bonds of the electron orbitals of carbon atoms in the structure of the tubes. The orbitals (s, p_x, p_y) combine to form in-plane σ (bonding or occupied) and σ_* (antibonding or unoccupied) orbitals. The lateral interaction with neighboring p_z orbitals (labeled the ppπ interaction) creates delocalized π (bonding) and π_* (antibonding) orbitals. In analogy, the σ bonds in the nanotube form a hexagonal network which strongly connects the carbon atoms in the cylinder wall of the CNT. The π bonds are perpendicular to the surface of the nanotube and are responsible for the weak interaction between SWNTs in a bundle, similar to the weak interaction between carbon layers of pure graphite [56].

The energy levels associated with the inplane σ bonds are known to be far away from the Fermi energy in graphite and thus do not play a key role in its electronic properties. In contrast, the bonding and antibonding π-bands cross the Fermi level at the high-symmetry points in the Brillouin zone of graphene [57].

The electronic structures of undoped single-walled CNT(3,3) and CNT(5,5) were calculated relatively long ago, and these low-diameter CNTs may be considered now as objects which are well-studied by various calculation methods [58–60].

The electronic structures of the low-diameter (i.e., with low values of m and n) B- or N-doped CNT(n,m) are also well-studied. In particular, such calculations were reported for the B(N)-doped metallic-type CNT(5,5) [61–63] and also for semiconductor-type B(N)-CNT(5,7) [64] and N-CNT(6,0) [65] and for many other B(N)-doped CNTs with higher values of (n,m). The electronic structures of B(N)-doped graphene sheets were studied recently within a molecular cluster approach by the DFT-based methods (see [66, 67]).

As it was found, doping of CNTs with the B or N impurities enhances their ability to absorb gaseous molecules [14, 15, 68]. This finding has roused an intense interest on the boron- and nitrogen-doped CNTs (B-CNTs and N-CNTs) as promising materials for gas sensors [14, 68, 69].

It is known that CNT(n,m) for which $n - m = 3l$ with l an integer (including armchair-type CNTs for which $m = n$) is characterized by the metallic-type electronic band-structure, whereas all other CNTs with $n - m = 3l \pm - 1$ are semiconductors [55]. Principle of operation of a CNT-based gas sensor is based on measurements of resistance of the working material. So, as the working material is a mixture of CNTs with dispersed (m,n), just the metallic-type CNTs should form conductivity properties of the mixture rather than semiconductor ones. Therefore, studies of armchair-type CNTs obviously should have higher priority.

It should be noted that the majority of modern synthesis procedures of CNTs allow to produce only mixes of CNTs with high dispersion of index (m,n) (see [70] and references therein). Technologies of synthesis of CNTs monodisperse by (m,n)

index (or procedures of selection of already synthesized CNTs by their structure) appeared only in the recent years and still are very complicated and expensive (see [71] and references therein). Sensing materials of existing CNT-based gas sensors are in fact "mixes" of CNTs with high dispersion of (*m*,*n*) index as these materials were produced by "conventional" synthesis methods without preliminary selection by the CNT structure (see [8, 18, 72]). Therefore, it is obvious that studies of a set of CNTs with various (*m*,*n*) indexes are desirable for prediction of properties of real working materials of the CNT-based gas sensors. However, studies of such a set require extensive computing resources and make analysis of results very complicated. So, researchers generally limit themselves to consideration of gaseous adsorption of the CNTs with some single case of (*m*,*n*) index [14, 17]) or graphene [18] reasonably regarding such limitation as being sufficient for adequate prediction of the physical properties of real gas sensing materials.

21.3 Modelling of Adsorption Properties of the CNT Surface by the DFT-Based Electronic Structure Calculations: A Brief Description of Computational Approach

21.3.1 Construction of CNT Clusters

The lengths of CNTs in mixtures may vary from several micrometers to hundreds of micrometers, and their diameters vary from nanometers to tens of nanometers [34]. Commercially available mixtures of carbon nanotubes consist mainly of MWCNTs with average diameters of 5 nm. The present-day computational capabilities are insufficient to perform a first-principle calculation for the full-length carbon nanotubes as well as for the entire variety of the nanotube structures.

The CNT(3,3) and CNT(5,5) are the narrowest possible nanotubes, with diameters of ~0.4 and ~0.7 nm, respectively. However, such nanotubes are convenient objects of calculations, since their clusters will have sufficient length for modeling of molecular adsorption even with relatively small number of atoms. A single-layered graphene sheet is commonly used to model the surface of large-diameter CNTs (with correspondingly, low surface curvature). Consideration of both low-diameter CNTs and graphene is a widely spread approach in prediction of the adsorption properties of real CNT mixtures by computational studies [73–75].

The CNTs and graphene were modeled in our calculations as molecular clusters. For calculations of adsorption of hydrogen halide molecules HX, the clusters of CNT(3,3) comprised 78 carbon atoms (or in other words, 13 C_6 "rings" along the nanotube axis) were taken. To compensate the effects of dangling C–C bonds, 12 outermost C atoms of the clusters were replaced by the H atoms providing $C_{66}H_{12}$ formula of the cluster. Such replacement is a widely used approach in computational modeling of CNTs within molecular cluster approach [69, 76, 77]. To model the

B or N impurities, one carbon atom from the central 6 "ring" of the cluster was substituted by the boron or nitrogen atom.

It should also be noted that the lengths of real CNTs usually exceed their diameters by several orders of magnitude. So, a "section" of the CNT modeled in a cluster must be long enough to provide a negligible influence of side surfaces on the central region of the section where the B(N) impurities and adsorbed HX molecules are adsorbed. To examine this property, we performed supplementary geometry-optimized calculations of undoped CNT(3,3), CNT(5,5), and graphene clusters. According to the supplementary calculations, addition of two extra carbon "rings" to both sides of CNT(3,3) and CNT(5,5) clusters only slightly (within 0.8% of magnitude) changes the C-C distances in the central regions of clusters. Analogous weak changes in the core region were observed when two extra carbon "strips" were added to the opposite sides of graphene cluster. The following characteristic size parameters of undoped CNT(3,3) cluster were obtained in geometry-optimized calculations: distance along the nanotube axis between outermost C_6 "rings" was 12.3 Å, distance between edging H_6 "rings" (clusterlength) was 14.1 Å, and averaged distance between "contralateral" C nuclei of the central C_6 "ring" (cluster diameter) was 4.2 Å. Analogously, the length and diameter of the undoped CNT(5,5) cluster were obtained as 14.2 and 7.0 Å, respectively. Characteristic dimension of undoped graphene cluster (the longest internuclear distances between the H nuclei located on the opposite sides) was obtained as ~11.74 × 13.6 Å, respectively.

Since molecular anions of M(VI) metals have sizes larger than the hydrogen halide molecules HX, molecular clusters of larger sizes were needed to calculate molecular anions adsorption simulations than for hydrogen halide. Therefore, for the calculation of adsorption of M(VI) molecular anions the clusters of CNT(3,3) comprising 23 C_6 "rings" of armchair CNT(3,3) was used. The dangling C–C bonds in the cluster were capped with H atoms, resulting in $C_{126}H_{12}$ formula (see Fig. 21.4a).

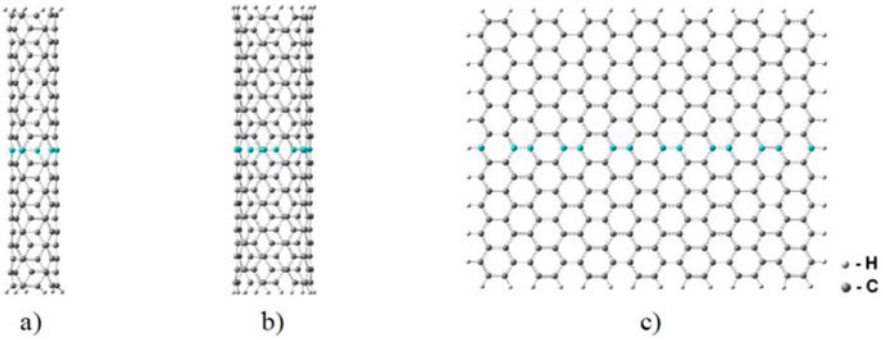

Fig. 21.4 Undoped clusters with optimized geometry: CNT(3,3) (**a**), CNT(5,5) (**b**), and graphene sheet (**c**)

Clusters with the formulas $C_{210}H_{20}$ and $C_{266}H_{46}$, respectively, were constructed to model a CNT(5,5) and graphene (see Fig. 21.4b, c, respectively). Approximate lengths of both CNT clusters were 26.5 Å. The dimensions of GR cluster were 24.1 × 30.8 Å.

Clusters of all undoped carbon nanostructures used in calculations were electrically neutral, while additional charges equal to $-1e$ and $+1e$ were assigned to clusters describing the B- and N-doped clusters, respectively. By using such additional charges, we have modeled a very common situation when an "additional" electron introduced into a real CNT by the N_C impurity is compensated by an additional charge $+1e$ of defect created somewhere far from the N_C site (such compensating defects were not modeled explicitly in our calculations). Correspondingly, additional compensating defects can supply one "missing" electron in the B_C case. Taking into account the $-2e$ charge of "free" $M(VI)O_4^{2-}$ anion, additional $-2e$ charges were assigned to the clusters of undoped adsorbent and chromate anion. So, additional charges of $-3e$ or $-1e$ were assigned to the B- or N-doped clusters, respectively. All systems were treated as closed-shell, that is, with no unpaired electrons.

Characteristic size parameters of undoped CNT(3,3) cluster used in calculations of adsorption of M(VI) anions were the following: distance along the nanotube axis between the outermost C_6 rings was ~24.7 Å, distance between outermost H6 rings (cluster length) was ~26.5 Å, mean distance between "contralateral" C nuclei of the central C_6 ring (cluster diameter) was ~4.21 Å. Analogously, the length and diameter of undoped CNT(5,5) cluster were ~26.5 and ~6.84 Å, respectively. Characteristic dimension of undoped GR cluster (the maximal internuclear distances between the H nuclei located on the opposite sides of the sheet) was ~24.1 × 30.8 Å. It should be noted that the lengths of real CNTs usually exceed their diameters by several orders of magnitude. So, a "section" of the CNT modeled in a cluster must be long enough to guarantee a negligible influence of side surfaces on the central region of the section where the B(N) impurities and adsorbed $M(VI)O_4^{2-}$ anion are situated. To examine this property, we have performed supplementary geometry optimization calculations of undoped CNT(3,3), CNT(5,5), and GR clusters. As the calculations showed, removal of the two outermost carbon rings from both edges of CNT(3,3) and CNT(5,5) clusters (or the two outermost carbon "strips" from GR cluster) changes the C-C distances in the central regions of clusters within 0.3%. Such slight changes ensure a negligible influence of the cluster edges on the calculated adsorption geometries. Consequently, the selected sizes of clusters were considered optimal, as larger clusters require more CPU time.

To complement these edge cases of the CNT surface curvatures by an intermediate one, we have additionally considered a fragment of the hexa-layered multiwalled carbon nanotube which can be denoted using formal rules as MWCNT(17,17)@(21,21)@(25,25)@(29,29)@(33,33)@(37,37) and will be mentioned in the following text as MWCNT. The outer diameter of such MWCNT is ~5.1 nm, which corresponds to an average tube diameter in commercially available mixtures of CNTs [34].

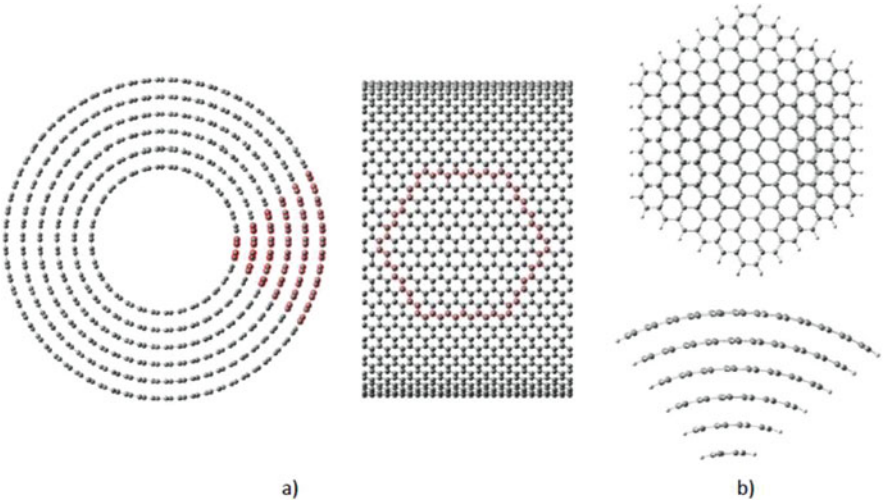

Fig. 21.5 (**a**) Scheme of selection of MWCNT cluster from six-walled carbon nanotube (edge atoms of the cluster are marked by red shadows); (**b**) structure of selected MWCNT cluster given in two projections

As it was found for the low-diameter CNTs [74], the nanotube fragments of at least 30 Å length can guarantee a sufficiently weak influence of the edges on the central part. However, construction of MWCNT cluster of such length would require 6800 carbon atoms. Such a number is too large for efficient DFT-based calculations of adsorption geometries, inasmuch as up to a 100s of combinations of adsorbents and adsorbates that have to be considered in our studies. For this reason, we have constructed a conical section of MWCNT which comprises a hexagonal part of the nanotube outer surface (for construction of the cluster, see Fig. 21.5). This part has transverse dimension of 29.0 Å, and the distance between inner and outer walls of MWCNT is 15.2 Å. All dangling C–C bonds of MWCNT cluster were capped by placement of H atoms providing a $C_{546}H_{126}$ formula.

During geometry optimization calculations, the H atoms of MWCNT cluster were fixed (frozen). As our geometry optimizations showed, the structure of MWCNT cluster was not stable without such freezing, that is, the carbon sheets constituting the conical part of the multiwalled tube moved apart. Normally, coaxial structure of MWCNTs prevents such decomposition. The freezing of the edge hydrogen atoms was applied in studies of molecular adsorption on the outer layer of MWCNT of 2 nm diameter [78]. Such freezing obviously provides some limitations to geometric optimization of the whole cluster. However, it leaves the atomic positions in the cluster core to be optimized thus providing (as it was also shown in [78]) an adequate treatment of molecular adsorption properties.

As a result, it was found that geometry optimization of undoped MWCNT cluster resulted in a little bulging of the outer carbon layers of the cluster (several deeper layers were also bulged but to a lower extent). However, despite the bulging, the

cluster preserved the curvature of the outer surface (after optimization, corresponding curvature radius decreased only by 10%). This feature shows that freezing of outer atoms provides a reasonable approximation in modeling of adsorption on medium-diameter MWCNT. An analogous approach to model the medium-diameter MWCNT has been successfully applied in [73].

21.3.2 Calculation Method, Basis Sets, and Other Computational Parameters

The geometry-optimized calculations were performed with use of Gaussian 09 [79] software package within density functional theory (DFT) level with B3LYP nonlocal correlation functional [80, 81]. The calculations used a basis set of 6-31G, which is typical for computational studies of adsorption of molecules (hydrogen halide) on the surface of CNT in recent years [69]. However, other base sets were used to calculate the molecular anions, since the heavy metals contained in the molecular anions are beyond the range that can be calculated using the base set of 6-31G. The basic set of cc-pVDZ was used for Cr and O atoms [82]. The atoms Mo and W are represented by the basis set of cc-pVDZ-PP with pseudo-potentials [83, 84]. Such combination of basis sets is generally utilized in computational studies of adsorption of molecules with d-metals on the CNT surfaces [85, 86]. All other settings were Gaussian 09 defaults, that is, no additional keywords were specified. Effects of water solvent on the studied adsorption properties were considered within the polarizable continuum model (PCM) [87].

As starting geometry, the HX (X = F, Cl, Br) molecules were put at 1.5 Å distance from the CNT surface in the vicinity of the B(N) atom, and the HAX bond was initially oriented parallel to the CNT axis. In the geometry optimization studies, several starting positions of $M(VI)O_4^{2-}$ (M(VI) = Cr, Mo, W) anions with respect to the carbon surface were considered for each adsorption case. In all cases, the anions were initially put in such a way that the shortest C/B/N-O distance lied between 1.5 and 2.2 Å. Using such initial geometry, we ensure binding of the anion particularly to the dopant atoms, not at just some other site of the doped CNT or graphene sheet.

Excited electronic states of CrO_4^{2-} anions in "free" and in adsorbed configurations were studied by the time-dependent DFT method (TD-DFT) method. In these calculations, the two-level ONIOM-2 approach in treatment of interatomic interactions was used [88]. The "adsorbent $+CrO_4^{2-}$ anion" system with optimized geometry was divided into two regions, the quantum mechanical (QM) and the molecular mechanical (MM). The QM region comprised the atoms of CrO_4^{2-} anion, while the MM region comprised all atoms of the adsorbent molecule (C and H) (see Fig. 21.6). The electronic embedding was used in order to take into account electrostatic interaction between the QM and MM regions, i.e., the atoms of the QM region were treated by TD-DFT calculations, while the atoms of the

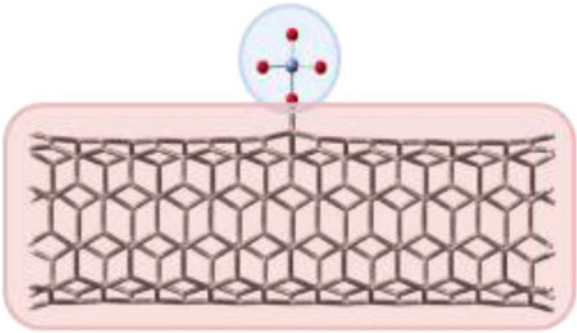

Fig. 21.6
Geometry-optimized structures of CNT(3,3) with adsorbed on the surface of CrO_4^{2-} anion are considered in the approximation of quantum mechanics (the region is painted blue), and CNT(3,3) is considered in the approximation of molecular mechanics (the region is painted with pink color)

MM region were treated as partial charges contributing to the quantum-mechanical Hamiltonian. Successful applications of the ONIOM approach to calculations of the excited states of molecules are reviewed in [89]. The TD-DFT is a well-established method for treatment of the excited states of tetrahedral oxyanions of d^0 metals (see [90] and references therein). The TD-DFT calculations of the singlet excited states of CrO_4^{2-} anions (QM region) were carried out in a single-point (no geometry optimization) calculation with the previously optimized geometry. The B3LYP exchange-correlation functional was used and only single excitations were taken into account. The same basis sets as for the geometry optimization calculations were used. Energies and oscillator strengths of electronic transitions from the ground to 50 lowest energy excited states were obtained.

21.4 Electronic Structure and Sensing Properties of Carbon Nanotubes with Adsorbed Hydrogen Halide Molecules HX (X = F, Cl, Br)

The results of geometry-optimized calculations of the electronic structure of carbon nanotubes (CNTs) and graphene (GR) with adsorbed HX (X = F, Cl, Br) are presented in this section. The influence of boron and nitrogen impurities on the formation and character of chemical bonds between carbon materials the molecules of halogen halides is analyzed.

The binding energies, E_b, were obtained as the difference of the calculated total energies using expression: $E_b = E_{\text{CNT-B(N)-HX}} - E_{\text{CNT-B(N)}} - E_{\text{HX}}$.

The calculated E_b value should be negative in a stable adsorption configuration. The charge states of HX (X = F, Cl, Br) adsorbates are obtained as an algebraic sum of calculated Mulliken charges of H and X atoms. Negative value of charge of the adsorbate molecule means transfer of negative electronic charge from the CNT to the molecule.

The calculated binding energies, charges on the HX adsorbate molecules (X = F, Cl, Br) and the optimized geometry of the internuclear distances of CNT(3,3), CNT(5,5) and graphene are presented in Table 21.1.

As Table 21.1 shows, our calculations provide relatively low values of binding energies between adsorbed HX (X = F, Cl, Br) molecules and undoped clusters: they range from −0.07 to −0.19 eV. Internuclear distances in adsorbed molecules $R_{H–X}$ are only slightly changed with respect to corresponding distances in free molecules (the difference does not exceed 1.5%). For all considered cases of adsorption on undoped clusters, the "axis" of HX molecule is settled practically perpendicular to the carbon surface. The shortest $R_{C–H}$ distance exceeds 2 Å for all studied HX cases.

For all adsorption configurations, calculations indicate lower binding energies and higher $(R_{C–H})^{min}$ distances for undoped graphene clusters in comparison with CNT(3,3) and CNT(5,5) (see Table 21.1). Values of E_b obtained for undoped CNT(3,3) and CNT(5,5) fall into the region of binding energies typical for hydrogen bonds (0.1–0.6 eV [91]) but are close to its lower limit. The E_b value in GR-HCl and GR-HBr cases are even slightly below this lower limit and fall into the region of the van der Waals bonds (0.01–0.1 eV, see [92]). Relatively low values of E_b and slight changes of internuclear distances in adsorbed molecules indicate the absence of covalent bonding between HX (X = F, Cl, Br) adsorbates and undoped carbon nanotubes.

Calculations also give low values for charges or HX molecules adsorbed on undoped clusters: they are in the −0.02 to −0.07 *e* range (see Table 21.1).

The calculated binding energies, charges on the HX adsorbate molecules (X = F, Cl, Br), and the optimized geometry of the internuclear distances of B-doped CNT(3,3), CNT(5,5), and graphene are shown in Table 21.2. In general, calculations show a completely different situation with respect to the adsorption of HX molecules on the surface of boron-doped carbon nanotubes in comparison with undoped nanostructures.

Calculations reveal far different situation for adsorption of HX molecules on the B-doped CNTs. In this case, the binding energies with adsorbate molecules range from −0.36 to −2.53 eV (see Table 21.2), and they are generally higher by an order of magnitude than corresponding energies of adsorption on undoped clusters. The E_b values for CNT(3,3) and CNT(5,5) definitely fall into the region of hydrogen bonds (0.1–0.6 eV, Ref. 202) or are slightly above this region [−0.87 eV, for CNT(3,3)-B-HCl], while the −2.13 eV value observed in CNT(3,3)-B-HBr case is typical for covalent bonds [93].

For CNT(5,5), all adsorption cases reveal lower binding energies relatively to CNT(3,3) (compare corresponding rows in Table 21.2). The B-doped graphene clusters reveal binding energies typical for covalent bonds (ranging from −2.53 for GR-B-HF to −2.38 for GR-B-HCl, see Table 21.2).

As Table 21.2 shows, in each case of HX adsorption on the B-doped CNT(3,3) and CNT(5,5), the H atom of the adsorbate is located closer to one of the atoms of the nanotube, than to the impurity atom B, that is, $(R_{C–H})^{min} < (R_{B–H})^{min}$. In the CNT(3,3)-B-HBr case, the $(R_{C–H})^{min}$ distance is even almost twice shorter than the $(R_{B–H})^{min}$ distance. So, it is arguable that C and H atoms create chemical bonds in

Table 21.1 Calculated binding energies, charges of adsorbate molecules HX (X = F, Cl, Br) and internuclear distances for undoped configurations

Type of adsorbate	Configuration	Binding energy E_b (eV)	Charge state of HX adsorbate (e)	$R_{H–X}/(R_{H–X})^{free}$	$(R_{C–H})^{min}$
HF	CNT(3,3)-HF	−0.19664	−0.038	0.9567/0.94927	2.07545
	CNT(5,5)-HF	−0.15972	−0.033	0.95255/0.94927	2.07033
	GR-HF	−0.1231	−0.024	0.95178/0.94927	2.24942
HCl	CNT(3,3)-HCl	−0.1356	−0.071	1.3404/1.32057	2.18253
	CNT(5,5)-HCl	−0.1422	−0.046	1.33027/1.32057	2.36785
	GR-HCl	−0.0707	−0.033	1.32667/1.32057	2.48136
HBr	CNT(3,3)-HBr	−0.1536	−0.068	1.4578/1.44006	2.20396
	CNT(5,5)-HBr	−0.16345	−0.044	1.44780/1.44006	2.36396
	GR-HBr	−0.0868	−0.031	1.44429/1.44006	2.46213

$R_{H–X}$(Å) – internuclear distance in adsorbed HX molecule
$(R_{H–X})^{free}$(Å) – internuclear distance in free HX molecule
$(R_{C–H})^{min}$(Å) – shortest distance from a carbon atom of the adsorbent to the H atom of HX

Table 21.2 Calculated binding energies, charges of adsorbate molecules HX (X = F, Cl, Br), and internuclear distances for the B-doped configurations

Type of adsorbate	Configuration	Binding energy E_b (eV)	Charge state of HX adsorbate (e)	$R_{H-X}/(R_{H-X})^{free}$	$(R_{C-H})^{min}$
HF	CNT(3,3)-B-HF	−0.5950	−0.03	0.9729/0.94927	1.90231
	CNT(5,5)-B-HF	−0.4963	−0.018	0.96624/0.94927	2.00599
	GR-B-HF	−2.5311	−0.003	0.9598/0.94927	2.24942
HCl	CNT(3,3)-B-HCl	−0.8800	−0.503	2.027/1.32057	1.15766
	CNT(5,5)-B-HCl	−0.3764	−0.137	1.37235/1.32057	1.96542
	GR-B-HCl	−2.3824	−0.12	1.35292/1.32057	2.56420
HBr	CNT(3,3)-B-HBr	−2.1342	−0.112	2.7779/1.44006	1.0962
	CNT(5,5)-B-HBr	−0.3622	−0.14	1.4933/1.44006	1.98348
	GR-B-HBr	−2.3907	−0.125	1.47253/1.44006	2.78799

R_{H-X}(Å) – internuclear distance in adsorbed HX molecule
$(R_{H-X})^{free}$(Å) – internuclear distance in free HX molecule
$(R_{C-H})^{min}$(Å) – shortest distance from a carbon atom of the adsorbent to the H atom of HX

all studied cases of adsorption on the B-doped CNT(3,3) and CNT(5,5) clusters. For the B-doped graphene, on contrary $(R_{C–H})^{min} > (R_{B–H})^{min}$ and the H atoms of the adsorbates create chemical bonds with the B dopants.

The most significant elongations of the H–X distances are obtained for CNT(3,3)-B-HBr and CNT(3,3)-B-HCl cases (∼53% and ∼93%, respectively). In contrast, adsorption of HX molecules on the B-doped graphene clusters, despite high binding energies, does not lead to significant changes of internuclear distances in the adsorbates (the relative change does not exceed 12.5%).

The calculated binding energies, charges on the HX molecules (X = F, Cl, Br), and the optimized geometry of the internuclear distances of N-doped CNT(3,3), CNT(5,5), and graphene are presented in Table 21.2.

In general, calculations show a situation similar to the case of adsorption of HX molecules on the surface of undoped clusters.

For all studied adsorptions cases, calculations give relatively low values of the binding energies (do not exceed −0.41 eV; see Table 21.3), small adsorbate charges (do not exceed |0.05| e), slight changes if internuclear distances in adsorbates (do not exceed 2.5%), and relatively high internuclear distances between the adsorbates and nanotubes (above 2 Å). Although for some cases (CNT(3,3)-N-HF, CNT(5,5)-N-HF, GR-N-HF, and CNT(5,5)-N-HBr) the values of E_b can be formally attributed to the energy range of weak hydrogen bonds (see above), the rest of the adsorption cases reveal binding energies typical for van der Waals' interaction (0.01–0.1 eV range of binding energies [92]), that is, physisorption.

Results of the study of the system "HX molecule (X = F, Cl, Br), adsorbed on the surface of undoped, B-, and N-doped CNT(3,3), CNT(5,5), and graphene" allow the following conclusions. The calculated binding energies and charges on adsorbates reveal the mechanism of physisorption of HX molecules on undoped graphene and undoped CNTs and on N-doped materials. Therefore, undoped, B-, and N-doped carbon nanotubes are less attractive to elaboration of sensors of hydrogen halide gases.

Materials based on the B-doped CNTs are perspective for sensing of HCl and HBr hydrogen halides as the molecules are chemisorbed on the nanotube surfaces.

21.5 Electronic Structure of Carbon Nanotubes with Adsorbed Molecular Anions of Hexavalent Metals and Perspectives for Removal of Toxic M(VI) Metals by Carbon Nanomaterials

This section presents calculation results and corresponding analysis for the electronic structure of single- and multiwalled carbon nanotubes and graphene with adsorbed anions of M(VI) metals. The influence of impurities (boron and nitrogen) and oxygen- and ammonia-containing functional groups on the formation of the interatomic bonds between carbon materials and the anions is analyzed in view of

Table 21.3 Calculated binding energies, charges of adsorbate molecules HX (X = F, Cl, Br), and internuclear distances for N-doped configurations

Type of adsorbate	Configuration	Binding energy E_b (eV)	Charge state of HX adsorbate (e)	$R_{H–X}/(R_{H–X})^{free}$	$(R_{C–H})^{min}$
HF	CNT(3,3)-N-HF	−0.1703	0.007	0.9555/0.94927	2.53622
	CNT(5,5)-N-HF	−0.4126	0.02	0.95049/0.94927	3.73704
	GR-N-HF	−0.2116	0.021	0.95008/0.94927	3.92233
HCl	CNT(3,3)-N-HCl	−0.0603	−0.064	1.3519/1.32057	2.66707
	CNT(5,5)-N-HCl	Geometry optimization unconverged			
	GR-N-HCl	−0.06534	−0.001	1.32000/1.32057	5.16923
HBr	CNT(3,3)-N-HBr	−0.0942	0.013	1.4392/1.44006	3.88017
	CNT(5,5)-N-HBr	−0.1868	−0.009	1.43967/1.44006	3.08926
	GR-N-HBr	−0.0716	0.005	1.43913/1.44006	4.17118

$R_{H–X}$(Å) – internuclear distance in adsorbed HX molecule
$(R_{H–X})^{free}$(Å) – internuclear distance in free HX molecule
$(R_{C–H})^{min}$(Å) – shortest distance from a carbon atom of the adsorbent to the H atom of HX

potential application of carbon nanomaterials for removal of M(VI) metals from air and water media.

The binding energies E_b of anions to adsorbents, both in vacuo and in aqua, were obtained as the difference of the calculated total energies using expression:

$$E_b = E_{ads-anion} - E_{ads} - E_{anion}, \tag{21.4}$$

where $E_{ads\text{-}anion}$ are total energies of the optimized adsorption system "adsorbent with anion," E_{ads} are total energies of the optimized adsorbent, and E_{anion} are total energies of optimized anions calculated within the same approximations.

Clusters of all undoped carbon nanostructures in calculations were electrically neutral, while additional charges equal to $-1e$ and $+1e$ were assigned to clusters describing the B- and N-doped clusters, respectively. Taking into account the $-2e$ charge of "free" $M^{VI}O_4^{2-}$ (M^{VI} = Cr, Mo, W) anion, additional $-2e$ charges were assigned to the clusters of undoped adsorbent and chromate anion. Consequently, additional charges of $-3e$ or $-1e$ were assigned to the B- or N-doped clusters, respectively.

Differences in charge density on the $M^{VI}O_4^{2-}$ (M^{VI} = Cr, Mo, W), $Cr_2O_7^{2-}$, and $HCrO_4^-$ anions (in respect to the isolated anion) in adsorbed state were defined as $\Delta q = -2e - q$ ($\Delta q = -e - q$ for $HCrO_4^-$), where q is an algebraic sum of charge states of all atoms of anion (calculated in adsorbed configuration using Mulliken population analysis). If the calculated value of Δq is negative, the electronic charge is transferred from the anion to the adsorbent.

21.5.1 Adsorption of $M(VI)O_4^{2-}$ (M(VI) = Cr, Mo, W) Anions on Undoped and B(N)-Doped CNTs

Single adsorption configurations were found in each case (see Fig. 21.7), except for the adsorption on undoped graphene.

In all cases, the binding energies are negative and fall within -0.5 to -7.2 eV range (Table 21.4). Such E_b values are typical for the chemisorption mechanism of adsorption [93].

All three anions, CrO_4^{2-}, MoO_4^{2-}, and WO_4^{2-}, have very similar dependencies of both E_b, and Δq on type of doping and type of the adsorbent structure. This feature is quite expected since Cr, Mo, and W metals are isoelectronic and the valence properties of $M(VI)O_4^{2-}$ anions are determined by interplaying $3d$ ($4d$ or $5d$) orbitals of the M(VI) cation and $2p$ orbitals of the oxygen ligands. At that, the cationic d orbitals are localized at the central core of the anion, so creation of the chemical bonds to outer atoms is determined mainly by the oxygen $2p$ orbitals which have very common energy and spatial structure for all three $M(VI)O_4^{2-}$ anions [90].

Two stable configurations (GR-1 and GR-2) were found for the case of the adsorption of $M^{VI}O_4^{2-}$ (M^{VI} = Cr, Mo, W) molecules on graphene sheet (Fig. 21.8).

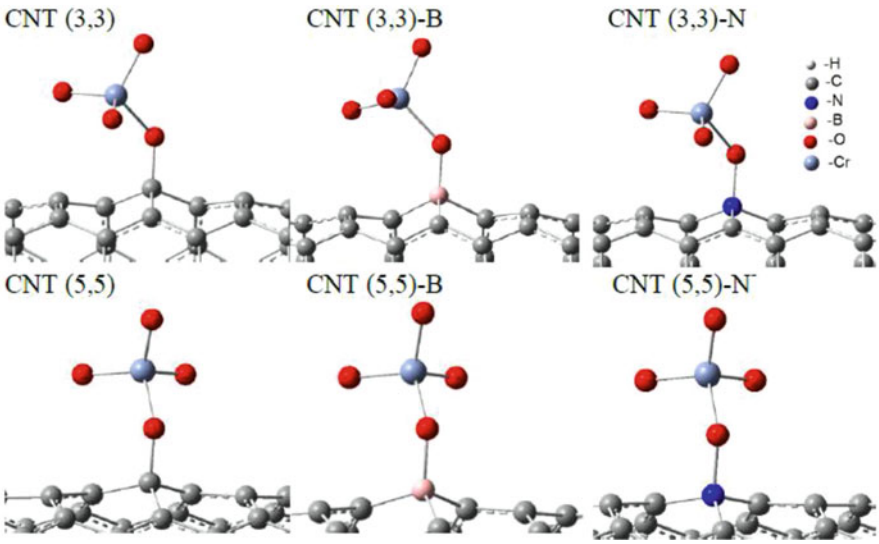

Fig. 21.7 Geometry-optimized structures of CrO_4^{2-} anions adsorbed on CNT(3,3) and CNT(5,5) in vacuo (only central parts of the clusters are shown)

So, our results indicate that one would expect quite similar absorption characteristics for the three anions and also for other types of adsorbents; for this reason we have limited the set of anions to only CrO_4^{2-} in studies of adsorption on the functionalized carbon nanostructures.

The optimized geometries of CrO_4^{2-} adsorbed on pristine and doped graphene (Fig. 21.8) illustrate typical peculiarities of adsorption configurations.

As Fig. 21.8 shows, in configuration 1 (such kind of atomic configuration is the most common among all adsorption cases), the chemical bond between the O atom of the anion and C atom of the adsorbent is created (the internuclear distance R_{C-O}^{min} is 1.47 Å which is a typical value for C–O covalent bonding [94]).

In configuration 2 (see Fig. 21.8), three O atoms are located at approximately equal distance from the carbon surface, that is, one of the faces of the CrO_4^{2-} tetrahedron is parallel to the graphene surface. In this configuration, each of the three O atoms is located about 2.80 Å above the center of C_6 "honeycomb" of graphene surface, and all three O atoms have approximately the same local surrounding. Within this accuracy, the structure is characterized by the C_3 symmetry axis perpendicular to the graphene plane and containing one C atom of the adsorbent, the Cr atom, and the "upper" O atom of the CrO_4^{2-} anion.

In the GR-B-CrO_4^{2-} case, one O atom of the anion creates a covalent bond to the boron dopant of the adsorbent (Fig. 21.8), and such kind of bonding is common for all cases of adsorption on the B-doped adsorbents. The situation is different for the N-doped adsorbents: one O atom of the anion can create bond either with N atom or with C atom which is the nearest neighbor to N (see Fig. 21.7 and 21.8).

Table 21.4 Binding energies E_b (eV), charge differences Δq (e) of $M(VI)O_4^{2-}$ (M(VI) = Cr, Mo, W) anions adsorbed on undoped and B(N)-doped carbon nanostructures, and the shortest internuclear distances R^{min} between anions and adsorbents (Å) calculated in vacuo

Configuration	E_b	Δq	R^{min}(bond type)
CNT(3,3)-CrO_4^{2-}	−3.79083	−0.8291	1.4161 (C–O)
CNT(5,5)-CrO_4^{2-}	−3.7329	−0.8974	1.43652 (C–O)
MWCNT-CrO_4^{2-}	−2.63828	−0.9464	1.45463 (C–O)
GR-CrO_4^{2-}-1	−2.89096	−0.9723	1.4678 (C–O)
GR-CrO_4^{2-}-2	−2.87873	−0.8554	3.14651 (C–O)
CNT(3,3)-B-CrO_4^{2-}	−0.76203	−0.5907	1.44814 (B–O)
CNT(5,5)-B-CrO_4^{2-}	−1.36138	−0.6446	1.47594 (B–O)
MWCNT-B-CrO_4^{2-}	−0.85638	−0.7705	1.50932 (B–O)
GR-B-CrO_4^{2-}	−1.50437	−0.8147	1.51794 (B–O)
CNT(3,3)-N-CrO_4^{2-}	−6.25441	−1.1137	1.48069 (N–O)
CNT(5,5)-N-CrO_4^{2-}	−5.62802	−1.119	1.51974 (N–O)
MWCNT-N-CrO_4^{2-}	−6.54564	−0.9901	1.39640 (C–O)
GR-N-CrO_4^{2-}	−6.79154	−0.9940	1.40748 (C–O)
CNT(3,3)-MoO_4^{2-}	−3.35158	−0.7910	1.42157 (C–O)
CNT(5,5)-MoO_4^{2-}	−3.23772	−0.8594	1.44191 (C–O)
GR-MoO_4^{2-}-1	−2.37352	−0.9282	1.47396 (C–O)
GR-MoO_4^{2-}-2	−2.34263	−0.7462	3.10782 (C–O)
CNT(3,3)-B-MoO_4^{2-}	−0.5478	−0.5701	1.45440 (B–O)
CNT(5,5)-B-MoO_4^{2-}	−1.05357	−0.6156	1.47825 (B–O)
GR-B-MoO_4^{2-}	−0.78632	−0.9420	1.55429 (C–O)
CNT(3,3)-N-MoO_4^{2-}	−5.61597	−1.0815	1.48592 (N–O)
CNT(5,5)-N-MoO_4^{2-}	−7.21026	−0.9307	1.40001 (C–O)
GR-N-MoO_4^{2-}	−6.49465	−0.9589	1.42121 (C–O)
CNT(3,3)-WO_4^{2-}	−3.23703	−0.7827	1.42612 (C–O)
CNT(5,5)-WO_4^{2-}	−3.12088	−0.8412	1.44547 (C–O)
GR-WO_4^{2-}-1	−2.27914	−0.9033	1.48033 (C–O)
GR-WO_4^{2-}-2	−2.36037	−0.7513	3.10519 (C–O)
CNT(3,3)-B-WO_4^{2-}	−0.53325	−0.5699	1.45440 (B–O)
CNT(5,5)-B-WO_4^{2-}	−1.01168	−0.6051	1.47534 (B–O)
GR-B-WO_4^{2-}	−1.10752	−0.7515	1.52304 (B–O)
CNT(3,3)-N-WO_4^{2-}	−5.42915	−1.0719	1.50997 (N–O)
CNT(5,5)-N-WO_4^{2-}	−7.07997	−0.9122	1.4075 (C–O)
GR-N-WO_4^{2-}	−6.21075	−0.9324	1.42828 (C–O)

Creation of covalent O-C bonds is observed for adsorption of CrO_4^{2-} and MoO_4^{2-} on CNT(3,3)-N and CNT(5,5)-N and for WO_4^{2-} on CNT(3,3)-N. The O-N covalent bonds are created in all other adsorption cases on the N-doped adsorbents. As Table 21.4 shows, creation of O-N bonds provides the highest absolute values of binding energies.

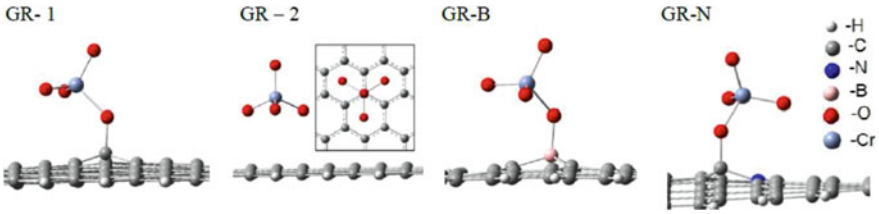

Fig. 21.8 Geometry-optimized structures of CrO_4^{2-} anions adsorbed on graphene in vacuo (only central parts of the clusters are shown)

The calculated oscillator strengths of CrO_4^{2-} anions are given in Fig. 21.9. As can be seen from the figure, calculations predict appearance of additional red bands of optical absorption of CrO_4^{2-} anions after on N-doped CNT. Such an appearance can be related to the fact that adsorption of CrO_4^{2-} on the N-doped CNT is accompanied by significant distortions of the anion nuclei. When considering distances and angles for adsorption on carbon nanostructures (see Table 21.5), one can see that the most significant distortions of the CrO_4^{2-} geometry are observed for adsorption on nitrogen-doped structures in comparison with undoped and B-doped configurations.

Since our results reveal the chemisorptions mechanisms, they indicate that the CNT-based materials can efficiently adsorb CrO_4^{2-}, MoO_4^{2-}, and WO_4^{2-} anions in gaseous media, i.e., from air atmosphere. However, the situation is quite different for adsorption in water.

The binding energies (E_b) and the charge difference (Δq) for the adsorbed configurations of $M(VI)O_4^{2-}$ on the surface of undoped, boron-nitrogen-doped, carbon nanostructures calculated *in aqua* are shown in Fig. 21.10.

As Fig. 21.10 shows, much lower absolute values of binding energies are observed for all studied combinations relatively to corresponding cases in vacuo. The E_b values of all adsorption cases on MWCNT cluster and graphene are positive indicating that adsorption of $M(VI)O_4^{2-}$ anions by such adsorbents is energetically unfavorable. Positive are also the energies of adsorption cases on all undoped adsorbents. Only the B- and N-doped CNT(3,3) and CNT(5,5) reveal negative E_b values and these values are below -2 eV for adsorption of CrO_4^{2-} and MoO_4^{2-} on CNT(3,3). All three anions reveal no stable adsorption configurations *in aqua* on undoped graphene, i.e., geometry optimization was not convergent.

From these results, we can conclude that undoped CNTs could be less-efficient materials for adsorption of $M(VI)O_4^{2-}$ anions in water. The efficiency can be improved if the materials would contain a valuable amount of low-diameter CNTs, or they would be doped by aliovalent impurities like B or N. Both ways of improvement are expensive and hardly realizable for massive production of CNT mixtures [96, 97]. So, another mechanism should be proposed to explain a substantial uptake of Cr(VI) anions by CNT-based materials from water solutions observed in experiments [36, 38, 98, 99]. These mechanisms are examined in the following subsection.

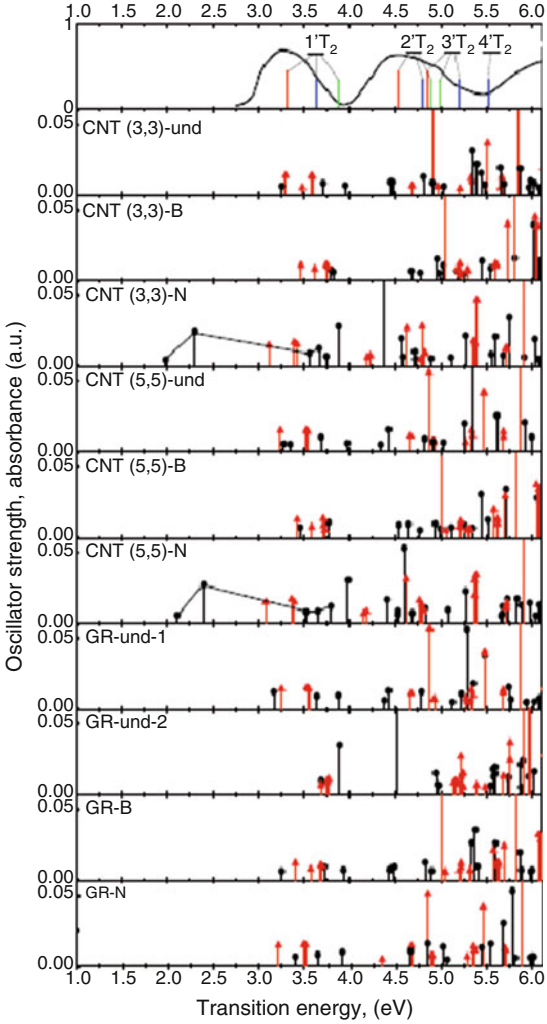

Fig. 21.9 Top plot: calculated energies of electronic transitions from the ground ($^1A_1$) to the low-energy excited states of free CrO_4^{2-} anions (blue bars); energies of the same transitions calculated with another basis sets [90] (green bars) and determined experimentally (red triangles); experimental absorption spectrum of chromate anion in aqueous solution (black solid line) [95]. Other plots: oscillator strengths of electronic transitions of CrO_4^{2-} anions adsorbed on the surface of carbon nanostructures calculated with (black circles) and without (red triangles) account of influence from the adsorbents

Table 21.5 Characteristic parameters of distortions of adsorbed CrO_4^{2-} anions

Configuration	Relative standard deviation of distances (%)	Relative standard deviation of angles (%)
CNT(3,3)-CrO_4^{2-}	6.3	2.1
CNT(5,5)-CrO_4^{2}	6.8	2.3
GR-CrO_4^{2-}	1.7	2.1
CNT(3,3)-B-CrO_4^{2-}	4.8	1.3
CNT(5,5)-B-CrO_4^{2}	5.1	1.5
GR-B-CrO_4^{2-}	5.3	1.6
CNT(3,3)-N-CrO_4^{2-}	7.7	3.1
CNT(5,5)-N-CrO_4^{2}	7.9	3.2
GR- N-CrO_4^{2-}	7.0	2.4

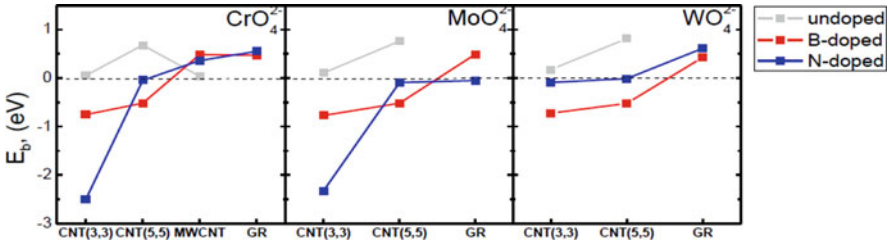

Fig. 21.10 Dependencies of binding energies E_b on adsorbent type and type of doping calculated in aqua

21.5.2 Adsorption of CrO_4^{2-} Anions on Functionalized CNTs

It is believed that one of the most efficient ways for enhancement of the adsorption capability of CNTs with respect to Cr(VI) compounds is functionalization of the CNT-based materials by the oxygen-containing surface functional groups (OSG) [2, 4, 34, 35]. In such functionalization, mixes of CNTs are treated by acids, for instance, by HNO_3 [34, 35] and then filtered, washed out, and dried up. As a result, various OSGs are created on the CNTs surfaces (a schematic explanation of the process can be found in [35]).

According to existing concepts [34, 36, 47], such kind of functionalization can enhance uptake of Cr(VI) compounds by the materials due to the following factors: (a) chemical reactions of Cr(VI) compounds with OSG can change the valence state of chromium ions Cr(VI) → Cr(III), whereas trivalent chromium ions are by several orders less toxic than hexavalent ones; (b) compounds of Cr(VI) can be chemically bound directly to atoms of OSG, that is, the groups can create additional adsorption cites for chromium compounds if compared with nonfunctionalized CNT surface; and (c) positively charged OSG^+ can be the centers of Coulomb attraction for negatively charged chromate anions like CrO_4^{2-} that enhances adsorption capability of functionalized CNT material (this concept is analyzed in [36]).

However, there were several experimental indications that Coulomb attraction to positively charged groups is a less important factor for enhancement of Cr(VI) uptake by the OSG-functionalized CNTs, and this enhancement occurs mainly due to creation of additional OSG-related adsorption sites [34]. In this subsection, we examine computationally, could the OSGs form such sites.

Particular objects of the calculations and motivation for their choice are the following. As it was shown in [35], the FTIR spectra of OSG functionalized CNT materials reveal spectral peaks corresponding to several oxygen-containing groups, in particular –OH (hydroxyl group), –COOH (carboxyl group), and $–COO^-$ (deprotonated carboxyl group). So, in our calculations we consider such groups and some of their combinations.

Here, we consider only one type of carbon nanotube, namely, CNT(5,5), since the main focus of the study is bonding of the anions to the OSGs, and the curvature of carbon surface is obviously expected to have a low importance.

The following functional groups are considered (see also Fig. 21.11):

1. CNT(5,5)-COOH. A neutral carboxyl group –COOH has one unpaired electron, whereas neutral cluster of CNT(5,5) has even number of electrons. An even number of electrons is a necessary condition for stability of the chemical bonds; so to model functionalization of the CNT by –COOH group, we assigned the $+1$e charge to CNT(5,5)-COOH adsorbent (accordingly, the -1e charge was assigned to CNT(5,5)-COOH-CrO_4^{2-} complex). So in fact we model a removal of an extra electron from the region of adsorption (from the OSG). Physically, this electron can be localized on some other defect in the CNT which is left beyond the study.
2. CNT(5,5)-B-COOH. Creation of B_C requires an extra electron, so it compensates the COOH group providing chemical stability for the complex. In this case, the adsorbent was taken electrostatically neutral, and correspondingly -2e charge was assigned to CNT(5,5)-B-COOH-CrO_4^{2-} system.
3. CNT(5,5)-COOH-OH. Carboxyl and hydroxyl groups are bound to two nearest C atoms of the nanotube. Unpaired electrons of both groups are mutually compensated, and such complex is considered as one of the most probable kings of coexistence of -COOH and -OH groups on the CNT surface (see [35] and references therein).

   As it was found experimentally [35, 36], adsorption capability of OSG-functionalized CNT materials with respect to Cr(VI) compounds in water solution substantially depends on the pH level. It is well-known that at high pH levels, OSG can be deprotonated (this process can be schematically denoted as $–COOH \rightarrow COO^- + H^+$ or $–OH \rightarrow –O^- + H^+$). To study the influence of deprotonation on adsorption of CrO_4^{2-}, we consider the following two complexes with deprotonated carboxyl groups:
4. CNT(5,5)-COO^--OH. Analogous to case (3) but with carboxyl group missing H^+ proton. The negative charge of carboxyl group is modeled by adding one extra electron, that is, assigning $-1e$ charge to the system.

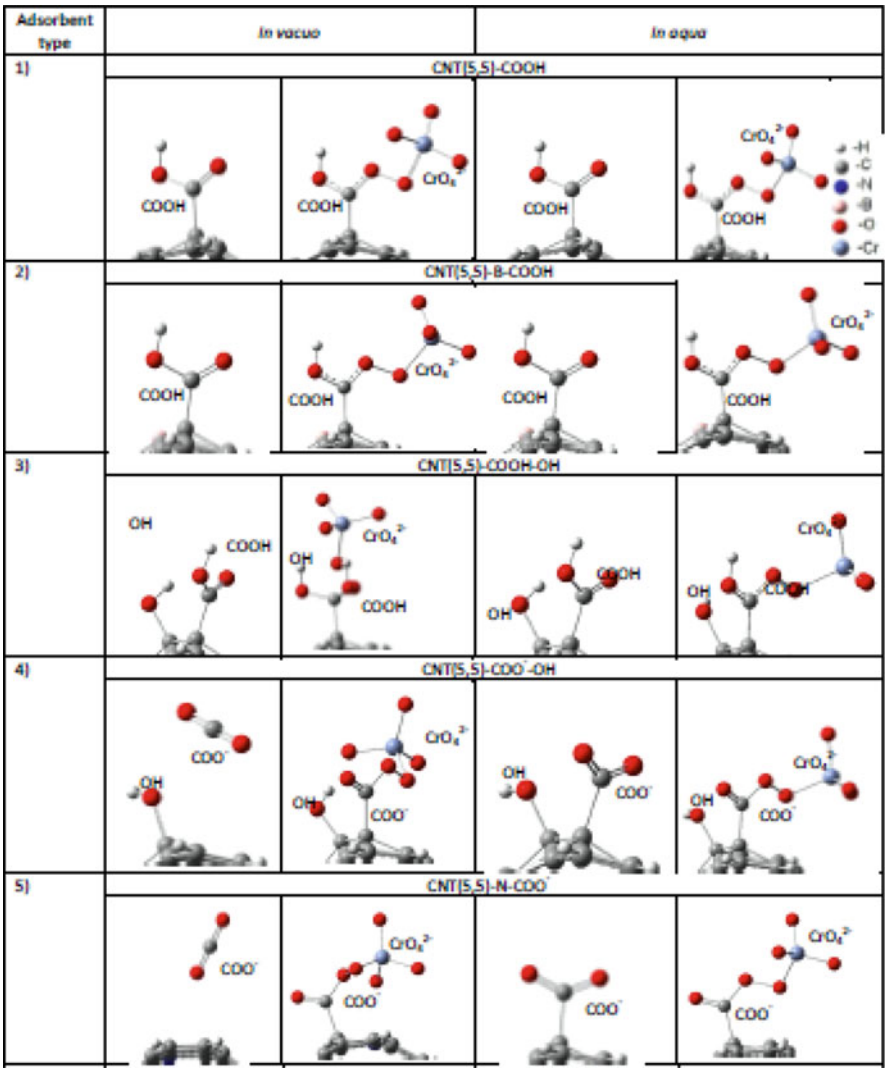

Fig. 21.11 Geometry-optimized structures of OSG-functionalized CNT(5,5) with (columns 2 and 4) and without (columns 1 and 3) adsorbed CrO_4^{2-} anions

5. CNT(5,5)-N-COO^-. The negative charge of carboxyl group is supplied by aliovalent impurity N_C.

   Functionalization of the CNTs by ammonia is a commonly applied method of influence on the adsorption properties of the CNT-based materials [76]. To study adsorption of CrO_4^{2-} on ammonia-functionalized CNTs, we consider the following cases:

Table 21.6 Binding energies E_b (eV), charge differences Δq (e) of CrO_4^{2-} anions adsorbed on functionalized CNT(5,5), and the shortest internuclear distances R^{min} between the anion and adsorbents (Å) calculated in vacuo

Type of adsorbent	E_b	Δq	R^{min}(bond type)
1. CNT(5,5)-COOH	−5.09424	−1.27908	1.44011 (O–O)
2. CNT(5,5)-B-COOH	−2.03214	−1.23958	1.44219 (O–O)
3. CNT(5,5)-COOH-OH	−4.15042	−1.04078	1.43590 (O–O)
4. CNT(5,5)-COO^--OH	–	−1.08516	1.44225 (O–O)
5. CNT(5,5)-N-COO^-	–	−1.14172	1.44671 (O–O)
6. CNT(5,5)-OH-NH_3^+	–	−0.6631	0.97521 (H–O) 1.60492 (H–O)
7. CNT(5,5)-1-NH_3^+	−10.53795	−0.57807	0.98510 (H–O) 1.99308 (H–O)
8. CNT(5,5)-2-NH_3^+	−10.30772	−0.5677	0.98504 (H–O) 2.0149 (H–O)

6. CNT(5,5)-OH-NH3$^+$. The ammonia –NH_3^+ and hydroxyl –OH groups are bound to the neighboring C atoms of the nanotube providing even number of electrons.
7. CNT(5,5)-1-NH_3^+ (1 = $C_8H_{16}O_2N$ = -C_2H_4-N-CH_2-CH_2-O-CH_2-CH_2-O-CH_2-CH_2-). Such kind of functionalization with ammonia can substantially enhance hydrophilicity of the CNT-based materials [100], even when functionalization procedures are rather complex [76, 101].
8. CNT(5,5)-2-NH3+ (2 = C_4H_8N = -C_2H_4-N-CH_2-CH_2-). Another group with NH_3^+ at the end, however, with different (approximately, a half-shorter) atomic chain between ammonia and the nanotube. Such shorter chain represents an intermediate case of distance between the NH_3^+ and the CNT surface if compared with corresponding distances in groups (6) and (7).

Calculation results on adsorption of CrO_4^{2-} anions on functionalized CNTs both in vacuo and *in aqua* are given in Table 21.6. As the calculations show, adsorbents (4), (5), and (6) are not stable in vacuo without CrO_4^{2-} anions (geometry optimizations unconverged), so the corresponding binding energies cannot be calculated.

As Table 21.6 shows for adsorbents (1)–(5), in all these cases, the R^{min} distances are typical for the covalent bonding between two oxygen atoms, that is, the anions are bound to the OSG by O-O covalent bonds both in vacuo and in aqua. At that, the R^{min} distances for in-vacuum and in-water adsorption on adsorbents (1)–(5) are very close (they differ by only few thousandths of Å); however, the binding energies E_b are significantly different. For vacuum, the E_b energies are negative, whereas for water they are positive, indicating that adsorption on adsorbents (1)–(5) in vacuo is energetically unfavorable.

Adsorption configurations of CrO_4^{2-} on adsorbents (7) and (8) in vacuo are characterized by the binding energies (near −10 eV) which are substantially higher

Table 21.7 Binding energies E_b (eV), charge differences Δq (e) of CrO_4^{2-} anions adsorbed on functionalized CNT(5,5), and the shortest internuclear distances R^{min} between the anion and adsorbents (Å) calculated *in aqua*

Type of adsorbent	E_b	Δq	R^{min}(bond type)
1. CNT(5,5)-COOH	3.67783523	−1.17828	1.44335 (O–O)
2. CNT(5,5)-B-COOH	3.76432267	−1.13843	1.44124 (O–O)
3. CNT(5,5)-COOH-OH	3.9323826	−1.15227	1.43907 (O–O)
4. CNT(5,5)-COO^--OH	2.28683293	−0.99205	1.44092 (O–O)
5. CNT(5,5)-N-COO^-	1.61844338	−1.02606	1.44856 (O–O)
6. CNT(5,5)-OH-NH_3^+	−0.92044761	−0.17524	1.70045 (H–O)
7. CNT(5,5)-1-NH_3^+	−1.00481	−0.19679	1.66845 (H–O)
8. CNT(5,5)-2-NH_3^+	−0.97787	−0.18121	1.70959 (H–O)

than E_b values of other adsorption configurations on functionalized CNTs found in vacuo (cases (1)–(3); see Table 21.6).

A distinctive feature of these configurations is that two O-H bonds between the anion and NH_3^+ group are created. One of them has R^{min} distance (0.985 Å) typical to covalent O–H bonding. However, the H atom of this bond lies closer to the anion than to the N atom of NH_3^+ group (corresponding H-N distance is 2.004 Å, whereas other H-N distances in the group are in the range 1.2–1.3 Å). So, attached to CNT surface OSGs of (1), (2), and (3) types as well as ammonia-containing groups (7) and (8) can be the centers of efficient adsorption of CrO_4^{2-} anions in vacuo.

The negative E_b values (about −1 eV) are also obtained for *in aqua* adsorption of CrO_4^{2-} on ammonia-functionalized CNTs (cases (6)–(8)). In each of these three cases, two O-H bonds between the oxygen atoms of the anion and the hydrogen atoms of NH_3^+ groups are created (correspondingly, two values are given in the R^{min} column of Table 21.7 for cases (6)–(8)). Such R^{min} values are typical for the hydrogen-type bonds [94].

So, taking into account generally weak adsorption of CrO_4^{2-} on undoped and B(N)-doped carbon nanostructures, it can be concluded that functionalization by ammonia-containing functional groups can enhance the adsorption capability of the CNT-based materials with respect to CrO_4^{2-} anions in water surrounding.

21.5.3 *Adsorption of $HCrO_4^-$ and $Cr_2O_7^{2-}$ Anions on Pristine, B(N)-Doped, and Functionalized Carbon Nanostructures*

Results obtained in Sect. 5.1 definitely indicate that almost all adsorption cases of $M(VI)O_4^{2-}$ anions on MWCNT reveal E_b, Δq, and R_{C-O}^{min} values which are intermediate between CNT(5,5) and graphene cases, both in vacuo and *in aqua*. This result implies that considering only two absorbents representing the "edge" cases of the nanotube surface curvature [CNT(5,5) and graphene] may provide

Table 21.8 Binding energies E_b (eV), charge differences Δq (e) of $HCrO_4^-$ and $Cr_2O_7^{2-}$ anions adsorbed on undoped and B(N)-doped carbon nanostructures, and the shortest internuclear distances R^{min} between the anions and adsorbents (Å) calculated in vacuo

Type of anion	Type of adsorbent	E_b	Δq	R^{min}(bond type)
$HCrO_4^-$	CNT(5,5)	−0.36325	−0.07179	3.06261 (C–O)
	CNT(5,5)-B	Unconverged		
	CNT(5,5)-N	−2.22284	−0.14129	2.99330 (C–O)
	GR	−0.34054	−0.07392	3.22327 (C–O)
	GR-B	Unconverged		
	GR-N	−2.04522	−0.0942	2.99330 (C–O)
$Cr_2O_7^{2-}$	CNT(5,5)	−1.37037	−0.32272	2.71228 (C–O)
	CNT(5,5)-B	0.092683	−0.46276	1.51208 (B–O)
	CNT(5,5)-N	−5.78497	−0.82444	1.43616 (C–O)
	GR	−0.87035	−0.78919	1.54294 (C–O)
	GR-B	0.175954	−0.59377	1.55506 (B–O)
	GR-N	−4.67928	−0.26619	2.77642 (C–O)

Table 21.9 Binding energies E_b (eV), charge differences Δq (e) of $HCrO_4^-$ and $Cr_2O_7^{2-}$ anions adsorbed on undoped and B(N)-doped carbon nanostructures, and the shortest internuclear distances R^{min} between the anions and adsorbents (Å) calculated *in aqua*

Type of anion	Type of adsorbent	E_b	Δq	R^{min}(bond type)
$HCrO_4^-$	CNT(5,5)	−0.0351	0.024866	3.94411 (C–O)
	CNT(5,5)-B	−0.09661	0.015293	3.95882 (C–O)
	CNT(5,5)-N	−0.10812	0.007237	3.22034 (C–O)
	GR	0.005776	0.00764	3.97388 (C–O)
	GR-B	0.027164	0.009331	3.97438 (C–O)
	GR-N	−0.01816	0.006586	3.95648 (C–O)
$Cr_2O_7^{2-}$	CNT(5,5)	−0.03814	0.036403	3.85276 (C–O)
	CNT(5,5)-B	−0.09642	0.038606	3.79722 (C–O)
	CNT(5,5)-N	−0.13169	0.013523	3.33032 (C–O)
	GR	0.01776	0.022416	3.96976 (C–O)
	GR-B	0.048613	0.03503	3.97388 (C–O)
	GR-N	−0.06209	0.003633	3.29386 (C–O)

quite sufficient information about adsorption properties with respect to oxoanions of hexavalent chromium. For this reason, we limit our studies of $HCrO_4^-$ and $Cr_2O_7^{2-}$ adsorption on undoped and B(N)-doped carbon nanostructures to only two types of adsorbents, namely, CNT(5,5) and graphene sheets.

As it follows from calculations (see Tables 21.8 and 21.9), adsorption of $Cr_2O_7^{2-}$ and $HCrO_4^-$ anions on undoped and B(N)-doped carbon nanostructures *in aqua* is characterized by either positive or nominally negative but very low in absolute values binding energies (not greater than |0.13| eV). Such E_b values, together with relatively long R^{min} (in 3.2–4 Å range; see Table 21.8), unambiguously reveal the absence of chemical bonding between the adsorbents and the anions. At that,

the cases with negative E_b values presented in Table 21.9 can be regarded as physisorption. Such results, together with results for adsorption of CrO_4^{2-} anion (see above) can lead to a conclusion that neither undoped nor B(N)-doped CNTs cannot by efficient adsorbents of the considered anions of hexavalent chromium in water surrounding.

However, adsorption configurations with chemical bonds and substantially negative binding energies exist in vacuo (see Table 21.8). As the table shows, the aliovalent doping of adsorbents in the case of $HCrO_4^-$ and $Cr_2O_7^{2-}$ adsorption has in general the same effect on the E_b values as it was in CrO_4^{2-} case (see above). Doping with N substantially lowers the E_b values (by ~2 and ~4 eV for $HCrO_4^-$ and $Cr_2O_7^{2-}$ adsorption, respectively) relatively to corresponding adsorption cases on undoped adsorbents. Doping with B, in contrast, leads to positive binding energies (in $Cr_2O_7^{2-}$ case) or to the absence of adsorbed configurations ($HCrO_4^-$ case).

Rather long R^{min} (near 3 eV; see Table 21.8) are obtained for all adsorption configurations of $HCrO_4^-$ in vacuo. At that, simultaneously, two [CNT(5,5)-N-$HCrO_4^-$ case] or even three (all other converged cases) oxygen atoms of $HCrO_4^-$ anion are located at approximately equal distance from the adsorbent.

Long R^{min} together with substantially negative E_b values are obtained in vacuo also for $Cr_2O_7^{2-}$ adsorption on CNT(5,5) and GR-N adsorbents. So, taking into account these results (and also results for CrO_4^{2-} presented above), we can conclude that carbon nanostructures will be efficient materials for removal of all three considered anions of Cr(VI) in gaseous state, whereby doping with N will enhance the adsorption capability of the materials.

Results for adsorption of $Cr_2O_7^{2-}$ and $HCrO_4^-$ anions on functionalized CNT(5,5) *in aqua* are presented in Table 21.10 (the adsorbents have the same notation as in Sect. 5.3) As Table 21.10 shows for both anions, all adsorbents

Table 21.10 Binding energies E_b (eV), charge differences Δq (e) of $HCrO_4^-$ and $Cr_2O_7^{2-}$ anions adsorbed on functionalized CNT(5,5), and the shortest internuclear distances R^{min} between the anion and adsorbents (Å) calculated *in aqua*

Type of adsorbate	Type of adsorbent	E_b	Δq	R^{min}(bond type)
$HCrO_4^-$	1. CNT(5,5)-COOH	−0.46465	−0.03652	1.62764 (H–O)
	2. CNT(5,5)-B-COOH	−0.38381	−0.01867	1.66788 (H–O)
	3. CNT(5,5)-COOH-OH	−0.11714	0.068841	2.64463 (C–H)
	4. CNT(5,5)-COO-OH	−0.77144	0.197648	1.6253 (H–O)
	5. CNT(5,5)-N-COO^-	2.714456	−0.13429	1.46669 (O–O)
	6. CNT(5,5)-OH-NH_3^+	−0.52561	−0.06348	1.84429 (H–O)
$Cr_2O_7^{2-}$	1. CNT(5,5)-COOH	−0.52714	−0.01422	1.63343 (H–O)
	2. CNT(5,5)-B-COOH	−0.44699	−0.0132	1.64909 (H–O)
	3. CNT(5,5)-COOH-OH	−0.35767	0.050108	1.80878 (H–O)
	4. CNT(5,5)-COO-OH	−0.1915	0.114867	3.78136 (O–O)
	5. CNT(5,5)-N-COO^-	2.581851	−0.49302	1.4541 (O–O)
	6. CNT(5,5)-OH-NH_3^+	−0.57704	−0.04804	1.83167 (H–O)

reveal adsorbed configurations with negative binding energies (in −0.1 to −0.6 eV range) excluding adsorbent (5), for which the energy is positive. For both anions on adsorbent (5), the R^{min} distances (Table 21.10) show O-O chemical bonding between oxygen atoms of the anions and functional group –COO^-.

However, significantly positive E_b values (above 2.5 eV) clearly indicate that adsorption on this adsorbent is energetically unfavorable. Adsorption of $HCrO_4^-$ on adsorbent (3) and adsorption of $Cr_2O_7^{2-}$ on adsorbent (4) do not lead to creation of chemical bonds between the anions and functional groups, whereas the absolute values of binding energies in these two cases are low (fall between −0.1 and −0.2 eV). So evidently, the physisorption mechanism is realized in both cases.

For the rest of configurations presented in Table 21.10, the O-H bonds between the anions and functional groups are created (even two O-H bonds are observed for ammonia-containing adsorbent (6)). Such results indicate that chemisorption mechanism is realized in all these cases.

So, our calculations show that $Cr_2O_7^{2-}$ and $HCrO_4^-$ anions can be efficiently adsorbed by the OSG and ammonia-functionalized carbon nanostructures in water.

Our results can explain the experimentally observed dependencies of Cr(VI) uptake by the OSG-functionalized CNT-based materials on pH level of water solution, which were presented in, for example [35]. The Cr(VI) uptake reaches the highest values when pH < 2, it decreases when 2 < pH < 6, and the Cr(VI) compounds are practically not adsorbed when pH > 6 [36]. It is known that at pH < 6 compounds of Cr(VI) exist predominantly as $Cr_2O_7^{2-}$ and $HCrO_4^-$, whereas at pH > 6 they exist as CrO_4^{2-} [35, 36]. Our results show that OSG-functionalized carbon nanostructures are good adsorbents of $Cr_2O_7^{2-}$ and $HCrO_4^-$ in water, while they poorly adsorb CrO_4^{2-}. So, the observed dependence of Cr(VI) uptake on pH level can be explained by this particular selectivity of the adsorbents with respect to the anions.

The above presented computational results and their analysis allow formulation of recommendations for functionalization of the CNT-based materials to enhance their adsorption capability with respect to Cr(VI) compounds in water. Functionalization of the materials both with OSG and ammonia-containing groups is feasible at low pH levels, whereas at high pH (>6), only functionalization by ammonia-containing groups will make sense. Undoped carbon nanostructures are poor adsorbents of Cr(VI) compounds in water, and aliovalent doping with B or N atoms does not improve the situation.

21.6 Conclusions

The results of the study of the system "HX molecule (X = F, Cl, Br), adsorbed on the surface of undoped, B-, and N-doped CNT(3,3), CNT(5,5) and graphene" clusters allow the following conclusions. The calculated binding energies and charges on adsorbates reveal the mechanism of physisorption of HX molecules on undoped graphene and undoped CNTs and on N-doped materials. Therefore, undoped, B-,

and N-doped carbon nanotubes are less attractive to elaboration of sensors of hydrogen halide gases. Materials based on the B-doped CNTs are perspective for sensing of HCl and HBr hydrogen halides as the molecules are chemisorbed on the nanotube surfaces.

The DFT-based electronic structure calculations predict that the CNT-based materials can efficiently adsorb $M^{VI}O_4^{2-}$ (M^{VI} = Cr, Mo, W), $Cr_2O_7^{2-}$, and $HCrO_4^-$ anions in gaseous surrounding. Doping of carbon nanostructures with nitrogen provides additional adsorption sites for the anions, so such kind of doping can enhance adsorption capability of the materials with respect to $M^{VI}O_4^{2-}$, $Cr_2O_7^{2-}$, and $HCrO_4^-$ anions.

Calculations predict that neither pristine nor B- or N-doped CNTs can be efficient adsorbents of $M^{VI}O_4^{2-}$ (M^{VI} = Cr, Mo, W), $Cr_2O_7^{2-}$, and $HCrO_4^-$ anions in water. Functionalization of CNTs by the ammonia-containing functional groups enhances their adsorption capability with respect to CrO_4^{2-}, $Cr_2O_7^{2-}$, and $HCrO_4^-$ anions in water, so such functionalization can enhance removal of Cr(VI) compounds from wastewaters by CNT-based materials. Functionalization of CNTs by the oxygen-containing functional groups does not enhance their adsorption capability in water with respect to CrO_4^{2-}; however it enhances adsorption of $Cr_2O_7^{2-}$ and $HCrO_4^-$ anions.

Acknowledgments The calculations were performed using Bem supercomputer of Wroclaw Center for Networking and Supercomputing (grant no. 300).

References

1. Anjum M, Miandad R, Waqas M, Gehany F, Barakat MA (2016) Remediation of wastewater using various nano-materials. Arab J Chem. https://doi.org/10.1016/j.arabjc.2016.10.004
2. Gupta VK et al (2016) Study on the removal of heavy metal ions from industry waste by carbon nanotubes: effect of the surface modification: a review. Crit Rev Environ Sci Technol 46:93–118
3. Mohmood I et al (2013) Nanoscale materials and their use in water contaminants removal—a review. Environ Sci Pollut Res 20:1239–1260
4. Ren X, Chen C, Nagatsu M, Wang X (2011) Carbon nanotubes as adsorbents in environmental pollution management: a review. Chem Eng J 170:395–410
5. Rao GP, Lu C, Su F (2007) Sorption of divalent metal ions from aqueous solution by carbon nanotubes: a review. Sep Purif Technol 58:224–231
6. Mendoza F et al (2014) Room temperature gas sensor based on tin dioxide-carbon nanotubes composite films. Sensors Actuators B Chem 190:227–233
7. Fam DWH, Palaniappan A, Tok AIY, Liedberg B, Moochhala SM (2011) A review on technological aspects influencing commercialization of carbon nanotube sensors – ScienceDirect. Sensors Actuators B Chem 157(1):1–7
8. Wang Y, Yeow JTW (2009) A review of carbon nanotubes-based gas sensors. J Sensors. https://doi.org/10.1155/2009/493904
9. Mittal M, Kumar A (2014) Carbon nanotube (CNT) gas sensors for emissions from fossil fuel burning. Sensors Actuators B Chem 203:349–362
10. Lee K et al (2013) Highly sensitive, transparent, and flexible gas sensors based on gold nanoparticle decorated carbon nanotubes. Sensors Actuators B Chem 188:571–575

11. Ueda T, Katsuki S, Takahashi K, Narges HA, Ikegami T, Mitsugi F (2008) Fabrication and characterization of carbon nanotube based high sensitive gas sensors operable at room temperature. Diam Relat Mater 17(7–10):1586–1589
12. Kauffman DR, Star A (2008) Carbon nanotube gas and vapor sensors. Angew Chem Int Ed 47(35):6550–6570
13. Cazorla C (2015) The role of density functional theory methods in the prediction of nanostructured gas-adsorbent materials. Coord Chem Rev 300:142–163
14. Bai L, Zhou Z (2007) Computational study of B- or N-doped single-walled carbon nanotubes as NH3 and NO2 sensors. Carbon 45:2105–2110
15. Zhou Z, Gao X, Yan J, Song D (2006) Doping effects of B and N on hydrogen adsorption in single-walled carbon nanotubes through density functional calculations. Carbon 44:939–947
16. Villalpando-Páez F et al (2004) Fabrication of vapor and gas sensors using films of aligned CNx nanotubes. Chem Phys Lett 386:137–143
17. Wang R, Zhang D, Zhang Y, Liu C (2006) Boron-doped carbon nanotubes serving as a novel chemical sensor for formaldehyde. J Phys Chem B 110:18267–18271
18. Adjizian J-J et al (2014) Boron- and nitrogen-doped multi-wall carbon nanotubes for gas detection. Carbon 66:662–673
19. An W, Turner CH (2009) Electronic structure calculations of gas adsorption on boron-doped carbon nanotubes sensitized with tungsten. Chem Phys Lett 482:274–280
20. Talla JA (2012) Ab initio simulations of doped single-walled carbon nanotube sensors. Chem Phys 392:71–77
21. Vikramaditya T, Sumithra K (2014) Effect of substitutionally boron-doped single-walled semiconducting zigzag carbon nanotubes on ammonia adsorption. J Comput Chem 35:586–594
22. Anderson B et al (2005) Encyclopedia of toxicology, four-volume set: encyclopedia of toxicology, 2nd edn. Academic Press, Oxford, p 2000
23. Aylón E et al (2007) Emissions from the combustion of gas-phase products at tyre pyrolysis. J Anal Appl Pyrolysis 79:210–214
24. Hall WJ, Williams PT (2006) Pyrolysis of brominated feedstock plastic in a fluidised bed reactor. J Anal Appl Pyrolysis 77:75–82
25. Barontini F, Cozzani V (2006) Formation of hydrogen bromide and organobrominated compounds in the thermal degradation of electronic boards. J Anal Appl Pyrolysis 77:41–55
26. Karama JPB et al (2013) Modeling the emission of hydrogen chloride and free chlorine from the thermal treatment of polyvinyl chloride- (PVC-) based plastic materials. J Anal Appl Pyrolysis 101:209–214
27. Stavert DM, Archuleta DC, Behr MJ, Lehnert BE (1991) Relative acute toxicities of hydrogen fluoride, hydrogen chloride, and hydrogen bromide in nose- and pseudo-mouth-breathing rats. Fundam Appl Toxicol 16:636–655
28. https://www.sierramonitor.com/electrochemical-toxic-gas-sensor-module-5100-xx-it
29. Datta S, Vero SE, Hettiarachchi GM, Johannesson K (2017) Tungsten contamination of soils and sediments: current state of science. Current Pollution Rep 3:55–64
30. Halmi MIE, Ahmad SA (2014) Chemistry, biochemistry, toxicity and pollution of molybdenum: a mini review. J Biochem Microbiol Biotechnol 2:1–6
31. Wang C-W, Liang C, Yeh H-J (2016) Aquatic acute toxicity assessments of molybdenum (+VI) to *Daphnia magna*. Chemosphere 147:82–87
32. Jung C et al (2013) Hexavalent chromium removal by various adsorbents: powdered activated carbon, chitosan, and single/multi-walled carbon nanotubes. Sep Purif Technol 106:63–71
33. Tarutani N, Tokudome Y, Fukui M, Nakanishi K, Takahashi M (2015) Fabrication of hierarchically porous monolithic layered double hydroxide composites with tunable microcages for effective oxyanion adsorption. RSC Adv 5:57187–57192
34. Xu Y, Arrigo R, Liu X, Su DS (2011) Characterization and use of functionalized carbon nanotubes for the adsorption of heavy metal anions. New Carbon Mater 26:57–62

35. Hu J, Chen C, Zhu X, Wang X (2009) Removal of chromium from aqueous solution by using oxidized multiwalled carbon nanotubes. J Hazard Mater 162:1542–1550
36. Ihsanullah FA et al (2016) Effect of acid modification on adsorption of hexavalent chromium (Cr(VI)) from aqueous solution by activated carbon and carbon nanotubes. Desalin Water Treat 57:7232–7244
37. Pillay K, Cukrowska EM, Coville NJ (2009) Multi-walled carbon nanotubes as adsorbents for the removal of parts per billion levels of hexavalent chromium from aqueous solution. J Hazard Mater 166:1067–1075
38. Verdugo EM, Xie Y, Baltrusaitis J, Cwiertny DM (2016) Hematite decorated multi-walled carbon nanotubes (α-Fe_2O_3/MWCNTs) as sorbents for Cu(II) and Cr(VI): comparison of hybrid sorbent performance to its nanomaterial building blocks. RSC Adv 6:99997–100007
39. Ihsanullah FA et al (2016) Heavy metal removal from aqueous solution by advanced carbon nanotubes: critical review of adsorption applications. Sep Purif Technol 157:141–161
40. Emsley J (2011) Nature's building blocks: an A-Z guide to the elements. Oxford University Press, Oxford
41. Tytłak A, Oleszczuk P, Dobrowolski R (2015) Sorption and desorption of Cr(VI) ions from water by biochars in different environmental conditions. Environ Sci Pollut Res 22:5985–5994
42. Palmer CD, Wittbrodt PR (1991) Processes affecting the remediation of chromium-contaminated sites. Environ Health Perspect 92:25–40
43. Opperman DJ, Heerden E v (2007) Aerobic Cr(VI) reduction by Thermus scotoductus strain SA-01. J Appl Microbiol 103:1907–1913
44. Shouman MA, Fathy NA, Khedr SA, Attia AA (2013) Comparative biosorption studies of hexavalent chromium ion onto raw and modified palm branches. Adv Phys Chem. https://doi.org/10.1155/2013/159712
45. Dakiky M, Khamis M, Manassra A, Mer'eb M (2002) Selective adsorption of chromium(VI) in industrial wastewater using low-cost abundantly available adsorbents. Adv Environ Res 6:533–540
46. Romero-González J, Peralta-Videa JR, Rodríguez E, Ramirez SL, Gardea-Torresdey JL (2005) Determination of thermodynamic parameters of Cr(VI) adsorption from aqueous solution onto *Agave lechuguilla* biomass. J Chem Thermodyn 37:343–347
47. Kotaś J, Stasicka Z (2000) Chromium occurrence in the environment and methods of its speciation. Environ Pollut 107:263–283
48. Boulding JR (1996) EPA environmental assessment sourcebook. CRC Press, Boca Raton, Florida, USA
49. Iijima S (1991) Helical microtubules of graphitic carbon. Nature 354:56–58
50. Oberlin A, Endo M, Koyama T (1976) Filamentous growth of carbon through benzene decomposition. J Cryst Growth 32:335–349
51. Tennent HG (1987) Carbon fibrils, method for producing same and compositions containing same. *U.S. Patent No. 4,663,230*. Washington, DC: U.S. Patent and Trademark Office.
52. Iijima S, Ichihashi T (1993) Single-shell carbon nanotubes of 1-nm diameter. Nature 363:603–605
53. Saito R (1998) Raman spectra of carbon nanotubes. In: Physical properties of carbon nanotubes. Published by Imperial College Press and distributed by World Scientific Publishing Co., pp. 183–206. https://doi.org/10.1142/9781860943799_0010
54. Ajayan PM et al (1993) Opening carbon nanotubes with oxygen and implications for filling. Nature 362:522–525
55. Charlier J-C, Blase X, Roche S (2007) Electronic and transport properties of nanotubes. Rev Mod Phys 79:677–732
56. Charlier JC (1991) First-principles study of the electronic properties of graphite. Phys Rev B 43:4579. Available at: https://journals.aps.org/prb/abstract/10.1103/PhysRevB.43.4579. Accessed 1 Dec 2018

57. Reich S, Thomsen C, Maultzsch J (2008) Carbon nanotubes: basic concepts and physical properties. Wiley, Hoboken, New Jersey, USA
58. Bertoni G, Calmels L (2006) First-principles calculation of the electronic structure and energy loss near edge spectra of chiral carbon nanotubes. Micron 37:486–491
59. Borštnik U, Hodošček M, Janežič D, Lukovits I (2005) Electronic structure properties of carbon nanotubes obtained by density functional calculations. Chem Phys Lett 411:384–388
60. Ito A, Natsume Y, Ohmori S, Tanaka K (2002) Electronic structures of very thin carbon nanotubes: are they still π-electronic materials? Nano Lett 2:629–633
61. Boutko VG, Gusev AA, Shevtsova TN, Pashkevich YG (2011) Structural and electronic properties of single-wall carbon nanotubes with various nitrogen content. Low Temp Phys 37:1021–1025
62. Wang K, Shi C, Zhao N, Du X, Li J (2009) First-principles study of the B- or N-doping effects on chemical bonding characteristics between magnesium and single-walled carbon nanotubes. Chem Phys Lett 469:145–148
63. Buonocore F (2007) Doping effects on metallic and semiconductor single-wall carbon nanotubes. Philos Mag 87:1097–1105
64. D'yachkov PN, Kutlubaev DZ, Makaev DV (2010) Linear augmented cylindrical wave Green's function method for electronic structure of nanotubes with substitutional impurities. Phys Rev B 82:035426
65. Esrafili MD (2013) Nitrogen-doped (6,0) carbon nanotubes: a comparative DFT study based on surface reactivity descriptors. Comput Theor Chem 1015:1–7
66. Zhang L, Xia Z (2011) Mechanisms of oxygen reduction reaction on nitrogen-doped graphene for fuel cells. J Phys Chem C 115:11170–11176
67. Fazio G, Ferrighi L, Di Valentin C (2014) Boron-doped graphene as active electrocatalyst for oxygen reduction reaction at a fuel-cell cathode. J Catal 318:203–210
68. Talla JA (2012) First principles modeling of boron-doped carbon nanotube sensors. Phys B Condens Matter 407:966–970
69. Ghasemi AS (2013) A DFT computation for comparison of NQR of O_2, N_2 and CO over the surface of Single-Walled Carbon Nanotubes Res. J Appl Sci Eng Tech 5:1892
70. Hong G, Chen Y, Li P, Zhang J (2012) Controlling the growth of single-walled carbon nanotubes on surfaces using metal and non-metal catalysts. Carbon 50:2067–2082
71. Sanchez-Valencia JR et al (2014) Controlled synthesis of single-chirality carbon nanotubes. Nature 512:61–64
72. Valentini L et al (2003) Sensors for sub-ppm NO2 gas detection based on carbon nanotube thin films. Appl Phys Lett 82:961–963
73. Hizhnyi Y, Nedilko S, Borysiuk V, Shyichuk A (2018) Removal of oxoanions of MVI (MVI=Cr, Mo, W) metals by carbon nanostructures: insights into mechanisms from DFT calculations. Int J Quantum Chem 118:e25715
74. Hizhnyi Y, Nedilko S, Borysiuk V, Shyichuk A (2017) Ab initio computational study of chromate molecular anion adsorption on the surfaces of pristine and B- or N-doped carbon nanotubes and graphene. Nanoscale Res Lett 12:71
75. Hizhnyi Y, Nedilko SG, Borysiuk V, Gubanov VA (2015) Computational studies of boron- and nitrogen-doped single-walled carbon nanotubes as potential sensor materials of hydrogen halide molecules HX (X = F, Cl, Br). Int J Quantum Chem 115:1475–1482
76. Galano A (2006) On the influence of diameter and length on the properties of armchair single-walled carbon nanotubes: a theoretical chemistry approach. Chem Phys 327:159–170
77. Petrushenko IK, Ivanov NA (2013) Structural and electronic properties of finite-length single-walled carbon and silicon carbide nanotubes: DFT study. Mod Phys Lett B 27:1350210
78. Vasiliev I, del Puerto ML, Jain M, Lugo-Solis A, Chelikowsky JR (2009) Application of time-dependent density-functional theory to molecules and nanostructures. J Mol Struct THEOCHEM 914:115–129
79. Frisch MJ, Trucks GW, Schlegel HB, Scuseria GE, Robb MA, Cheeseman JR, Scalmani G, Barone V, Mennucci B, Petersson GA, Nakatsuji H, Caricato M, Li X, Hratchian HP, Izmaylov AF, Bloino J, Zheng G, Sonnenberg JL, Hada M, Ehara M, Toyota K, Fukuda R,

Hasegawa J, Ishida M, Nakajima T, Honda Y, Kitao O, Nakai H, Vreven T, Montgomery JA Jr, Peralta JE, Ogliaro F, Bearpark M, Heyd JJ, Brothers E, Kudin KN, Staroverov VN, Kobayashi R, Normand J, Raghavachari K, Rendell A, Burant JC, Iyengar SS, Tomasi J, Cossi M, Rega N, Millam JM, Klene M, Knox JE, Cross JB, Bakken V, Adamo C, Jaramillo J, Gomperts R, Stratmann RE, Yazyev O, Austin AJ, Cammi R, Pomelli C, Ochterski JW, Martin RL, Morokuma K, Zakrzewski VG, Voth GA, Salvador P, Dannenberg JJ, Dapprich S, Daniels AD, Farkas O, Foresman JB, Ortiz JV, Cioslowski J, Fox DJ (2009) Gaussian 09, Revision E.01. Gaussian, Inc., Wallingford

80. Becke AD (1993) A new mixing of Hartree-Fock and local density-functional theories. J Chem Phys 98:1372–1377
81. Lee C, Yang W, Parr RG (1988) Development of the Colle-Salvetti correlation-energy formula into a functional of the electron density. Phys Rev B 37:785–789
82. Dunning TH (1989) Gaussian basis sets for use in correlated molecular calculations. I. The atoms boron through neon and hydrogen. J Chem Phys 90:1007–1023
83. Peterson KA, Figgen D, Dolg M, Stoll H (2007) Energy-consistent relativistic pseudopotentials and correlation consistent basis sets for the 4d elements Y–Pd. J Chem Phys 126:124101
84. Figgen D, Peterson KA, Dolg M, Stoll H (2009) Energy-consistent pseudopotentials and correlation consistent basis sets for the 5d elements Hf–Pt. J Chem Phys 130:164108
85. Kumari I, Gupta S, Goel N (2016) A DFT based investigation of NO oxidation by (CrO3)3 cluster. Comput Theor Chem 1091:107–114
86. Zhai H-J, Li S, Dixon DA, Wang L-S (2008) Probing the electronic and structural properties of chromium oxide clusters (CrO3)n− and (CrO3)n (n = 1–5): photoelectron spectroscopy and density functional calculations. J Am Chem Soc 130:5167–5177
87. Boys SF, Bernardi F (1970) The calculation of small molecular interactions by the differences of separate total energies. Some procedures with reduced errors. Mol Phys 19:553–566
88. Dapprich S, Komáromi I, Byun KS, Morokuma K, Frisch MJ (1999) A new ONIOM implementation in Gaussian98. Part I. The calculation of energies, gradients, vibrational frequencies and electric field derivatives (Dedicated to Professor Keiji Morokuma in celebration of his 65th birthday). J Mol Struct THEOCHEM 461–462:1–21
89. Chung LW et al (2015) The ONIOM method and its applications. https://doi.org/10.1021/cr5004419
90. Seidu I, Krykunov M, Ziegler T (2015) Applications of time-dependent and time-independent density functional theory to electronic transitions in tetrahedral d0 metal oxides. J Chem Theory Comput 11:4041–4053
91. Minkin VI (1999) Glossary of terms used in theoretical organic chemistry. Pure Appl Chem 71:1919–1981
92. Israelachvili JN (1991) Intermolecular and surface forces, 2nd edn. Academic Press, London
93. Owen S, Hoeben P, Headlee M (2014) Chemistry for the IB diploma coursebook with free online material. Cambridge University Press, Cambridge, England, UK
94. Haynes WM (ed) (2014) CRC handbook of chemistry and physics. CRC Press, Boca Raton
95. Johnson LW, McGlynn SP (1970) The electronic absorption spectrum of chromate ion. Chem Phys Lett 7:618–620
96. Mercuri F, Baldoni M, Sgamellotti A (2012) Towards nano-organic chemistry: perspectives for a bottom-up approach to the synthesis of low-dimensional carbon nanostructures. Nanoscale 4:369–379
97. Ewels CP, Glerup M (2005) Nitrogen Doping in Carbon Nanotubes. J Nanosci Nanotechnol 5:1345–1363
98. Lee C-G, Kim S-B (2016) Cr(VI) adsorption to magnetic iron oxide nanoparticle-multi-walled carbon nanotube adsorbents. Water Environ Res 88(11):2111–2120. https://doi.org/10.2175/106143016X14733681695401
99. Bhaumik M, Agarwal S, Gupta VK, Maity A (2016) Enhanced removal of Cr(VI) from aqueous solutions using polypyrrole wrapped oxidized MWCNTs nanocomposites adsorbent. J Colloid Interface Sci 470:257–267

100. Dehghani MH et al (2015) Removal of noxious Cr (VI) ions using single-walled carbon nanotubes and multi-walled carbon nanotubes. Chem Eng J 279:344–352
101. Georgakilas V et al (2002) Amino acid functionalisation of water soluble carbon nanotubes. Chem Commun 0:3050–3051